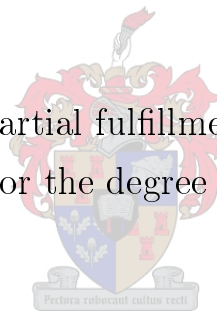


Generation and detection of ultrashort pulses

by

Victoria Onyeka Nwosu

Thesis presented in partial fulfillment of the requirements
for the degree of



Master of Science

at the University of Stellenbosch

Supervisor: Prof. E. G. Rohwer

Co-supervisors: Prof. H. Schwoerer and Dr. G. Arendse

March 2009

Declaration

By submitting this thesis electronically, I declare that the entirety of the work contained therein is my own, original work, that I am the owner of the copyright thereof (unless to the extent explicitly otherwise stated) and that I have not previously in its entirety or in part submitted it for obtaining any qualification.

03/03/2009.....

Date

Copyright © 2008 Stellenbosch University

All rights reserved

Abstract

The exciting field of ultrashort laser optics has experienced tremendous growth since its inception. One of its branches that has been of continuous interest is the characterization of ultrashort laser pulses. The need for complete characterization of these pulses has increased with applications in various fields of research.

Opto-electronic devices are incapable of resolving the temporal duration of these short optical pulses and other indirect techniques have been developed. Most self referencing techniques developed for short pulse characterization exploits the interaction of the input pulse with a copy of itself in a nonlinear medium.

This project studies the ultrashort optical regime. It explains the theory on autocorrelation pulse characterization techniques including the Spectral Phase Interferometry for Direct electric-field Reconstruction (SPIDER) technique. SPIDER measures the interference between a pair of replicas of the input pulse that has been spectrally sheared. A spectrometer is used to record the interferogram and the spectral phase is retrieved through a non-iterative, and purely algebraic method.

A SPIDER setup was constructed and used to measure femtosecond laser pulses. The SPIDER technique has the uniqueness of been a single shot, precise, reliable and self referencing diagnostics technique for ultrashort laser pulse characterization. It is also capable of retrieving the amplitude and phase of the input pulse. The input pulse measured revealed that the pulse duration is about 106 fs with a quadratic spectral phase implying a linear chirp on the pulse. (Numerical simulations were used to verify the algorithm).

Acknowledgements

My sincere gratitude goes to my supervisors Prof. E.G Rohwer, Prof. H. Schwoerer and Dr. G.J. Arendse for their enormous supervision, support and motivation.

Special thanks to Gurthwin Bosman for all the assistance he offered during the course of this work.

I would like to acknowledge all the members of the Laser Research Institute (LRI) for inspiration and support.

My profound gratitude to the African Institute for Mathematical Sciences (AIMS) and the African Laser Center for financial support.

I am indebted to my dear friends Florimond Mpiana, Emmanuel Jonah, Gibson Ikoro, Joy Okonkwo and Justin Mabilia for the love, support and constructive criticism they offered to me during the course of the work.

I will not forget to appreciate every member of my family, my parents, Lt. Colonel E.O Nwosu and Mrs H.N. Nwosu. My siblings, Marian, Jane, Augustine, Felix, and Daniel for their continual love and support.

Finally, I thank the almighty God for granting me favor and leading me this far.

Thank you all.

Contents

Abstract	i
List of Figures	ix
1 Introduction to ultrashort pulsed lasers	1
1.1 Historical development of the laser	1
1.2 Aim and outline of this work	3
1.3 Generating ultrashort pulses	3
1.3.1 Modelocking	4
1.3.2 Active modelocking	5
1.3.3 Passive modelocking	7
2 Interaction of light with solid materials	9
2.1 Significance of the generalized wave equation	9
2.2 Origin of dispersion in materials	11
2.3 Optical dispersion in materials	15
2.4 Ultrashort pulse propagation in a dispersive medium	16
3 Description of an ultrashort pulse	20
3.1 Temporal and spectral representations	20
3.2 Time bandwidth product	21
3.3 Variation of instantaneous frequency with time	23
4 Nonlinear optical processes	27
4.1 The origin of nonlinear polarization	28
4.2 Second harmonic generation (SHG)	34
4.3 Phase matching	35

5	Correlation techniques for ultrashort pulse characterization	39
5.1	Intensity autocorrelation	40
5.2	Interferometric Autocorrelation	41
6	Spectral Interferometry	50
6.1	Fourier Transform Spectral Interferometry	50
6.2	Principle of FTSI	51
6.3	Experimental results of FTSI	52
6.4	Spectral shearing interferometry	54
7	Spectral Phase Interferometry for Direct Electric Field Re- construction (SPIDER)	56
7.1	Optimization parameters	57
7.1.1	Generating the replica	57
7.1.2	Generating the chirped pulse	58
7.1.3	Nonlinear Interaction	60
7.2	SPIDER Theory	61
7.3	Experimental implementation, results and discussion	65
7.4	Numerical simulations	73
8	Conclusions	78
	Appendix	79
A		80
A.1	Gaussian pulse propagation through a medium	80
A.2	Conversion efficiency of the second harmonic wave	82
A.3	Matlab code for the phase retrieval	87
A.4	SPIDER verification algorithm	92

Bibliography

100

List of Figures

1.1	(a) Multimode and (b) Modelocked laser output	5
1.2	Frequency spectrum of an amplitude modulated field. Side band at $\omega_n \pm \Omega$ [1]	6
1.3	Transmission of a saturable absorber as a function of the incident intensity	8
2.1	Real part of the refractive index versus frequency	14
2.2	Imaginary part of the refractive index versus frequency	15
2.3	Dispersion curve for fused quartz	16
3.1	Temporal intensity of a Gaussian pulse with constant phase	21
3.2	Bandwidth limited Gaussian pulse	23
3.3	(a) Negatively chirped Gaussian pulse (b) Positively chirped Gaussian pulse	25
3.4	Illustration of the principle of chirped pulse amplification technique	26
4.1	Potential energy function for a nonlinear medium [2]	29
4.2	Schematic of the principle underlying second harmonic generation	34
4.3	Phase matching factor of the conversion efficiency for the second harmonic wave	37
4.4	Non-collinear geometry for phase matching, energy and momentum is conserved	38
5.1	Schematic of an intensity autocorrelator	41
5.2	Simulated intensity autocorrelation function for Gaussian shaped pulse	42

5.3	Schematic of an interferometric autocorrelator	42
5.4	Theoretical interferometric autocorrelation trace for a Gaussian shaped pulse with no chirp $\beta = 0$	48
5.5	Theoretical interferometric autocorrelation trace for a Gaussian shaped pulse with chirp parameter, $b = 2$	49
6.1	Schematic of a typical Fourier transform spectral interferometry set up	51
6.2	(a) Measured spectral interference for two replicas created from the reflection off an uncoated glass plate (b) Measured interference spectra of two frequency doubled replicas	52
6.3	(a) Inverse Fourier transform of (6.2) (b) Filtered positive side lobe	53
6.4	Phase transfer function retrieved for about $1.4 \mu\text{m}$ glass plate using FTSI	54
7.1	Basic components of a SPIDER set up	56
7.2	Schematic of a grating optical disperser used for stretching ultrashort pulses	58
7.3	Increase in the stretched pulse duration with grating pair separation	60
7.4	Schematic of the frequency shifting process used for the SPIDER technique	61
7.5	SPIDER inversion routine algorithm	65
7.6	Experimental layout of the SPIDER setup: IR-iris, GP-Glass plate, R-reflector, M-Mirrows, P-Gold coated right angled prism, T-translation stages, G-Gratings, L-Lens, BBO-Beta-barium borate nonlinear crystal	67
7.7	Input fundamental spectrum with Gaussian fit	68

7.8	Measured SPIDER interferogram (spidergram), phase information of the input pulse is converted to amplitude information	68
7.9	Inverse Fourier transform of the measured SPIDER interferogram. Side lobes are centred around the delay of the replicas	69
7.10	Measured calibration trace used for the inversion routine of the SPIDER interferogram	70
7.11	Fourier transform of the recorded calibration trace used in the SPIDER algorithm	70
7.12	Reconstructed spectral phase using integration (a) and concatenation methods (b)	71
7.13	Retrieved spectral intensity and spectral phase	72
7.14	Retrieved temporal profile and time dependent phase	73
7.15	Spectral phase returned by SPIDER (straight line) for an input pulse similar to that shown in figure 7.7, and the same pulse after propagating through a glass of 1 mm thickness (dots)	73
7.16	A picture of the SPIDER setup	75
7.17	Simulated SPIDER interferogram	76
7.18	Input (dash line) and reconstructed quadratic phase (solid line) using the SPIDER algorithm, $a = 5 \times 10^{-20} \text{ fs}^2$, $b = 0$, and $c = 0$	76
7.19	Input and reconstructed cubic phase using the SPIDER algorithm, $a = 0$, $b = 5 \times 10^{-56} \text{ fs}^2$, and $c = 0$	77
7.20	Input and reconstructed quartic phase using the SPIDER algorithm, $a = 0$, $b = 0$, and $c = 5 \times 10^{-71} \text{ fs}^2$	77

List of Tables

3.1	Values of time-bandwidth constants C for selected pulse shapes	23
5.1	Mathematical results for different pulse shapes and their correlation function [3]	41

1. Introduction to ultrashort pulsed lasers

1.1 Historical development of the laser

It is interesting to know that as diverse as the field of ultrashort laser optics is today, it all sprang up from basic physics principles. In this section we will give a brief discussion on the history of short pulse lasers and the development of ultrashort pulse characterization. The principle of laser operation was first discovered in 1916, when the great physicist Albert Einstein described the theory of stimulated emission. Before that time, the interaction of a photon with a molecule was explained with the principle of spontaneous emission and absorption. The former process occurs when a molecule is excited to a higher energy state, but does not remain there, it decays to a lower energy state and in the process emits a photon that has the energy corresponding to the energy difference between the two states. Absorption is the reverse process, where a molecule already in a lower energy state is raised to a higher energy state if it interacts with a photon that has the energy corresponding to the energy difference between the two states [4]. The interesting process on which the laser operates is stimulated emission where a molecule in a higher energy state interacts with a photon and decays to a lower energy level if the photon has the energy corresponding to the energy difference between the two states. The molecule emits a photon with the same direction, energy and phase as the photon that stimulated the process. After the description of the theory of stimulated emission by Einstein, it was used for several practical applications. However it was not until 1960 that Theodore Maiman utilized this principle and invented the first laser using a lasing medium of ruby crystal of aluminum oxide (Al_2CO_3) doped with chromium stimulated by high energy flashes of intense light. The laser had a fluctuating intensity lasting between a microsecond and a millisecond [5]. Shortly after that, in 1961 Hellwart proposed and implemented the concept of Q-switching. A giant pulse

of about 10 nanosecond was produced by Q-switching a ruby laser using a Kerr-cell shutter. The introduction of these Q-switched lasers with the high intensities they produce gave rise to the studies of various interesting nonlinear optical effects. To obtain shorter pulses, modelocking of a large number of longitudinal modes activated by the gain profile of the lasing medium was proposed by Hagrove, Fork and Pollack in 1964 [5]. Pulses shorter than a nanosecond were obtained by DeMaria et al. in 1966 by passive modelocking of a Nd-glass laser, which has a broad gain profile [5]. Today, modelocking based on transition-metal-doped crystals such as Ti:Sapphire have been optimized to produce ultrashort pulses of a few femtoseconds. As these pulses become shorter, their use for fundamental studies and applications increases rapidly. The ability to measure them also becomes increasingly important [6]. Measuring these pulses involves, determining the pulse width, the spectral intensity and phase or in time domain the temporal profile and phase of the ultrashort pulse. There are several important aspects of short pulse measurement. First, a precise knowledge of the pulse properties is necessary to verify the theoretical models of pulse creation. Secondly, in order to make even shorter pulses, it is necessary to understand the distortions that limit the length of the currently available pulses. Thirdly, in experiments using these short pulses, it is always important to know at least the pulse duration in order to determine the temporal resolution of a given experiment [6]. Pulse shaping experiments however requires the complete characterization of the shaped pulse [7, 8]. The technology for measuring ultrashort pulses must pace up with the lasers themselves [9]. Traditional correlation techniques only provide information about the pulse width after an assumption of the pulse shape [10]. With techniques such as Frequency Resolved Optical Gating (FROG) and Spectral Phase Interferometry for Direct Electric field Reconstruction (SPIDER) it is possible to measure pulses over a wide range of wavelengths, pulse durations and retrieve the amplitude and phase of the pulse. This leads us to the aim and outline of this work.

1.2 Aim and outline of this work

The main aim of this project work is to discuss the principle of the SPIDER technique, define the design considerations and experimentally implement the technique for laser pulse characterization. This thesis is split into 8 chapters, in chapter one we introduce historical development, motive and concepts used for ultrashort pulse generation. Chapter two explains some interesting phenomena of the interaction of light with solids. In chapter three we give a theoretical description of an ultrashort pulse. Chapter four focuses on the origin and considerations of nonlinear optics. In chapter five, we introduce the concept of pulse characterization and discussed some traditional correlation techniques for pulse measurement. In chapter six we introduced the concept of spectral interferometry and explained how the concept has been previously used to obtain phase information of an ultrashort pulse. Chapter seven covers the main focus of this work. The SPIDER principle is explained, the experimental design considerations are explained and the numerical and experimental results discussed.

1.3 Generating ultrashort pulses

There are some basic components necessary to generate an ultrashort pulse. Firstly, it requires a broad gain bandwidth medium to be pumped by a source. This requirement is a result of the inverse Fourier relationship between frequency and time, in order to obtain a short pulse in time, a broad frequency spectrum is required. Titanium: Sapphire (Al_2O_3) has shown to be an excellent gain medium for laser operation in the near infrared region. Its broad gain bandwidth (from 660-1100 nm) allows for a large tuning range and is well suited for ultrashort pulse generation [11]. Although a broad spectrum is necessary for ultrashort pulse generation, it is not sufficient. One can find a thermal source or an LED that has the same frequency spectrum as a 10 fs visible pulse. The spectral intensity only provides information about the relative spectral intensities or spectral modes that compose the light but

gives no information about the relative phases between these modes [12]. For ultrashort pulse generation there must be a well defined phases relation between these modes. Modelocking is an effective way of generating high intensity short pulsed lasers. Let us explain how this is achieved.

1.3.1 Modelocking

A typical laser cavity support the existence of longitudinal modes separated by the frequency difference $\Delta\nu = c/2\eta L$, where η is the refractive index of the gain medium, L is the length of the cavity and c the speed of light. These longitudinal modes generally oscillate independently of each other and the phases of the modes are randomly distributed. When by some means, many longitudinal modes with fixed frequency difference in a laser resonator are forced to maintain fixed phase relationships with each other, there is constructive interference and a short pulse is formed. This is termed modelocking [13]. The total electric field in the laser cavity is the superposition of the fields of the various N longitudinal modes [14] and can be written as

$$E(t) = \sum_{n=1}^N E_n e^{i[(2\pi\nu_0 + 2\pi n\Delta\nu)t + \phi_n]} \quad (1.1)$$

where n is the mode number, ν_0 is the fundamental laser center frequency and ϕ_n is the phase of the n th mode. The output power of such a system with random phases is proportional to the square of the electric field (and in the time domain, the output constitutes of series of spikes see figure 1.1(a)). In a modelocked laser, where all the modes have a fixed phase and assuming all modes have the same amplitude, the intensity of such a laser can then be expressed as [15]

$$I(t) = E_0^2 \frac{\sin^2(N\Delta\nu t)}{\sin^2(\Delta\nu t)}. \quad (1.2)$$

Such a system allows a well defined pulsed output in time (see figure 1.1(b)), with a repetition rate $1/T$. Most significantly, for modelocked lasers, is the

individual pulse width is then given by [15]

$$\tau_p = \frac{T}{N} = \frac{1}{\Delta\nu N} \quad (1.3)$$

where $\frac{1}{\Delta\nu N}$ is the gain bandwidth of the laser and determines the pulse width.

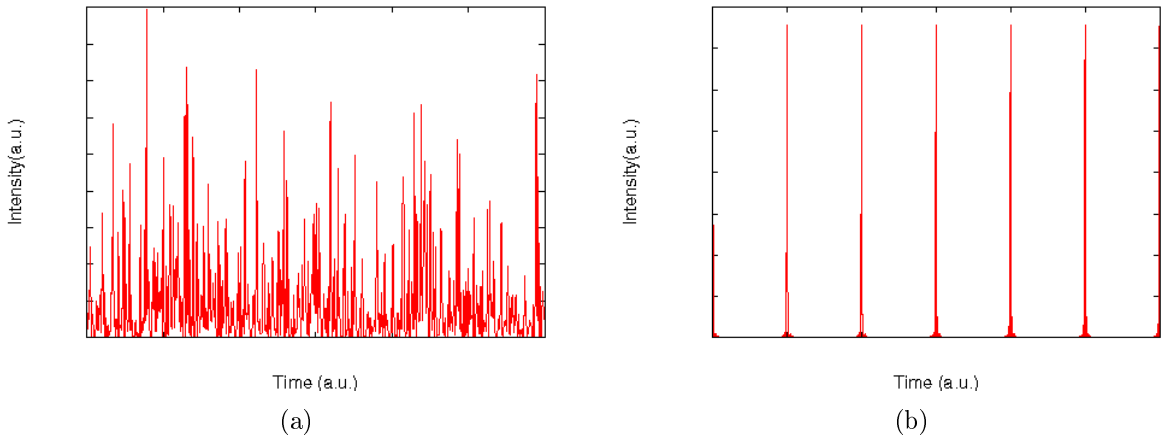


Figure 1.1: (a) Multimode and (b) Modelocked laser output

Practically modelocking is achieved either actively or passively or by the combination of both methods. Active modelocking involves placing an acoustic optic or electro-optic modulator in the cavity while passive modelocking involves the use of saturable absorber in the cavity [14]. Let us look at these concepts in detail.

1.3.2 Active modelocking

Active modelocking involves using an external modulator such as an acousto optical crystal or an electro optic modulator, a short pulse is generated if the modulation is synchronized with the cavity round trip frequency $c/2nL$. An amplitude modulation at the angular frequency Ω of the longitudinal modes results in the generation of side bands of angular frequency $\omega_n \pm \Omega$ (see figure 1.2) such that the side bands are displaced from the carrier frequency ω_n by Ω . Of particular interest is the case where the modulation frequency Ω is equal to the mode frequency spacing, that is

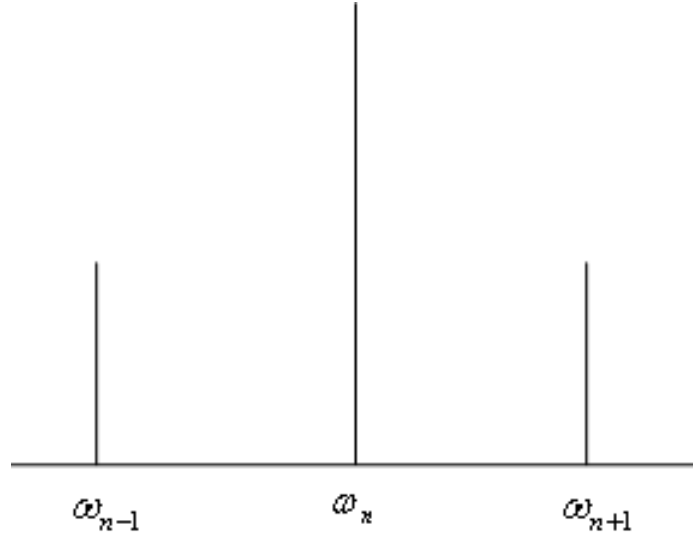


Figure 1.2: Frequency spectrum of an amplitude modulated field. Side band at $\omega_n \pm \Omega$ [1]

$$\Omega = \omega_{n+1} - \omega_n = 2\pi c/2nL \quad (1.4)$$

In such a situation, the side band of each mode exactly matches the frequencies of the adjacent mode, in this case each mode strongly couples with its nearest neighbors and this leads to a global phase locking over the whole spectral distribution. If the amplitude modulation is periodic, we can write the time dependence of mode n of frequency ω_n as [3]

$$E_n(t) = \varepsilon_n \cos(\omega_n t + \phi_n) [1 - \alpha(1 - \cos(\Omega t + \phi))] \quad (1.5)$$

where α is the modulation depth. Using trigonometrical identities equation (1.5) can be rewritten as

$$\begin{aligned} E_n(t) &= \varepsilon_n(1 - \alpha) \cos(\omega_n t + \phi_n) + \varepsilon_n \frac{\alpha}{2} \cos[(\omega_n - \Omega)t + \phi_n - \phi] \\ &+ \varepsilon_n \frac{\alpha}{2} \cos[(\omega_n + \Omega)t + \phi_n - \phi] \end{aligned} \quad (1.6)$$

So we see from equation (1.6) that an amplitude modulation generates side bands $\frac{\alpha}{2}$ times the carrier frequency amplitude. It is also evident from equation (1.6) that if the modulation frequency is driven at the frequency mode spacing, that is $\Omega = \omega_n \pm \omega_{n+1}$ then the side bands associated with each mode exactly coincide with the neighboring modes, resulting in the desired “locking” of all the modes.

1.3.3 Passive modelocking

The first optical pulses in the picosecond range was generated through passive modelocking. It utilizes the insertion of a saturable absorbing element inside the laser cavity. The absorption coefficient of the material is such that it can be saturated by high intensity, in other words it could reach a maximum transmission above the saturation intensity. As the gain medium is continuously pumped, at first the cavity loss is very large due to the absorber, the transmission of the absorber is almost constant at T_0 (figure 1.3) and independent of the incident intensity. Due to the large loss the laser can not oscillate and the gain in the medium increases. However, once the gain becomes high enough to overcome the losses in the cavity, the intensity in the cavity grows rapidly.

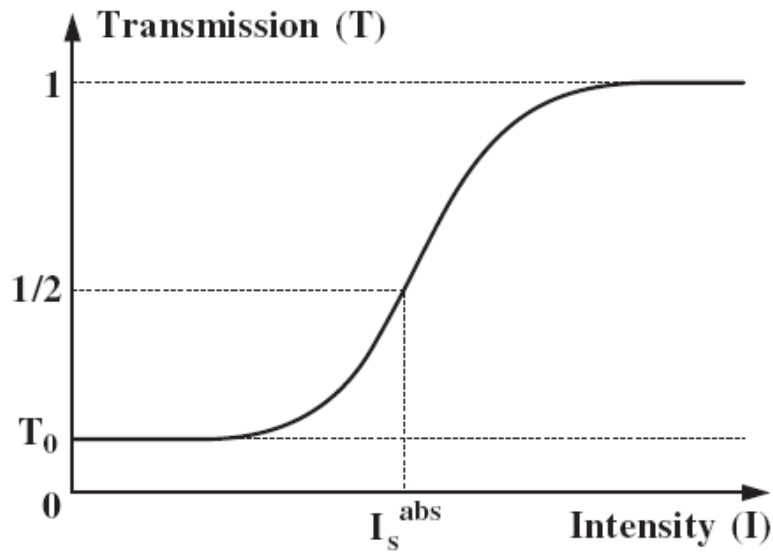


Figure 1.3: Transmission of a saturable absorber as a function of the incident intensity

At some saturation intensity I_s^{abs} the absorber becomes saturated, the cavity losses drop rapidly. This locks the modes together and the result is a short pulse in time [3].

2. Interaction of light with solid materials

In this chapter we will use the term “light” when relating to properties or effects of light in general, however we will be sure to use the term short pulses, or laser light when referring to effects that only the uniqueness of laser light can produce. Most optical experiments involve the propagation through or reflection of light from solid optical materials. The interaction of light with these solid materials result in interesting optical phenomena such as absorption, diffraction, emission, reflection, dispersion, and polarization effects [16]. The aim of this chapter will be to understand from a classical point of view the microscopic origin of some of the afore mentioned optical properties of solids. This is of relevance to this study because as we would see later, some of these effects are useful in ultrashort pulse characterization.

2.1 Significance of the generalized wave equation

If we consider only nonmagnetic, electrically neutral media, then this implies that the magnetization \mathbf{M} and volume density of electric charge ρ are zero in such media. The electromagnetic state of the medium can then be described by the polarization \mathbf{P} describing the response of the bound charges to the applied field and the current density \mathbf{J} describing the response of the conduction electrons to the applied field. The polarization \mathbf{P} is given by the expression

$$\mathbf{P} = (\epsilon - \epsilon_0) \mathbf{E} = \chi \epsilon_0 \mathbf{E} \quad (2.1)$$

where ϵ is the permittivity of the material and ϵ_0 is the permittivity of free space. The factor $\chi = \left(\frac{\epsilon}{\epsilon_0} - 1\right)$ is called the electric susceptibility and is

a unique property of the material. This expression for the polarization is only valid for isotropic materials such as glass where χ is a scalar quantity and has the same value for any direction of the applied field. Also the linear relationship between the polarization and electric field is correct under the approximation that the incident electric field is not high enough to consider higher order terms. As we will see later in chapter 4 if the electric field is high enough then the polarization must be expressed as a power series in the electric field. For now, we will treat the linear case. We begin by deriving the wave equation for an electric field in a medium. Maxwell's equations for the electric field \mathbf{E} and magnetic field \mathbf{H} are given by [17]

$$\nabla \times \mathbf{E} = -\mu_0 \frac{\partial \mathbf{H}}{\partial t} \quad (2.2)$$

$$\nabla \times \mathbf{H} = \epsilon_0 \frac{\partial \mathbf{E}}{\partial t} + \frac{\partial \mathbf{P}}{\partial t} + \mathbf{J} \quad (2.3)$$

$$\nabla \cdot \mathbf{E} = -\frac{1}{\epsilon_0} \nabla \cdot \mathbf{P} \quad (2.4)$$

$$\nabla \cdot \mathbf{H} = 0 \quad (2.5)$$

The general wave equation for the electric field is derived by taking the curl of equation (2.2) and the time derivative of equation (2.3). This gives

$$\nabla \times (\nabla \times \mathbf{E}) + \frac{1}{c^2} \frac{\partial^2 \mathbf{E}}{\partial t^2} = -\mu_0 \frac{\partial^2 \mathbf{P}}{\partial t^2} - \mu_0 \frac{\partial \mathbf{J}}{\partial t} \quad (2.6)$$

The two terms on the right hand side of equation (2.6) are called source terms and arise from polarization and conduction charges within the medium. For a nonconducting medium only the polarization term is important and is responsible for optical effects such as dispersion (which we will look at in detail), frequency conversion, and absorption. In the case of metals the conduction term is very important and is responsible for the opacity and high reflectance of metals. Now that we have an equation that describes the propagation of light in a medium. Our next interest is to understand the interactions of the field with the medium. In the next section, we will pay particular attention to absorption and dispersion as we would see later these two phenomena are very important in ultrashort optics and the SPIDER

technique in particular.

2.2 Origin of dispersion in materials

Considering nonconducting isotropic materials such as glass, we assume that the electrons behave as though the forces binding them to the nuclei are elastic forces described by Hooke's law. This means we are considering a linear response, where the restoring force is proportional to the displacement with opposite direction. We can use this idea to obtain an expression for the polarization in terms of the frequency of the applied field. The force on the electron due to the electric field is

$$\mathbf{F} = -e\mathbf{E} \quad (2.7)$$

Suppose each electron with charge $-e$ is displaced by a distance \mathbf{r} from its equilibrium position, then the resulting macroscopic static polarization of the medium is given by [16]

$$\mathbf{P} = -Ner = \frac{Ne^2}{K}\mathbf{E} \quad (2.8)$$

where N is the number of electrons per unit volume and K is the force constant. If the incident electric field is time dependent then the expression for polarization in equation (2.8) is incorrect, and the motion of the electrons must be considered. Considering the bound electrons as classical damped harmonic oscillators, the equation of motion for the electrons can be written as [16]

$$m\frac{d^2\mathbf{r}}{dt^2} + m\gamma\frac{d\mathbf{r}}{dt} + K\mathbf{r} = -e\mathbf{E} \quad (2.9)$$

where γ is the damping constant. Assume that the motion of the electrons has a harmonic time dependence such that a solution to the equation of motion in (2.9) would be $\mathbf{r} = \mathbf{r}_0 \exp(-i\omega t)$ where ω is the angular oscillation

frequency. Then solving equation (2.9) we get

$$(-m\omega^2 - i\omega m\gamma + K) \mathbf{r} = -e\mathbf{E} \quad (2.10)$$

and

$$\mathbf{r} = \frac{-e/m}{\omega_0^2 - \omega^2 - i\omega\gamma} \mathbf{E} \quad (2.11)$$

Using equation (2.8) and (2.11), the frequency dependent polarization can be written as

$$\mathbf{P} = \frac{Ne^2/m}{\omega_0^2 - \omega^2 - i\omega\gamma} \mathbf{E} \quad (2.12)$$

where we have used

$$\omega_0 = \sqrt{\frac{K}{m}}$$

as the effective resonance frequency of the bound electrons. As expected the polarization expression in equation (2.12) is the amplitude expression for a driven damped harmonic oscillator, so we expect to find some unique resonance phenomenon for frequency components close to the resonant frequency. This effect shows in the change of the index of refraction of the medium and strong absorption of light close to the resonant frequency. To show analytically how the polarization induces dispersion and absorption of light pulses, we go back to the general wave equation in (2.6), leaving out the conduction term because we are considering dielectric materials and substituting the expression for the polarization \mathbf{P} expressed in equation (2.12) into the wave equation. Since we are considering an isotropic medium, there is no variation of the effect of electric field on the medium, hence $\nabla \cdot \mathbf{E} = 0$ and the term $\nabla \times (\nabla \times \mathbf{E})$ equals $-\nabla^2 \mathbf{E}$ in equation (2.6). Then the polarization effect on the propagation of the pulse in the medium can be described by a simpler expression given by

$$\nabla^2 \mathbf{E} = \frac{1}{c^2} \left(1 + \frac{Ne^2}{m\epsilon_0} \cdot \frac{1}{\omega_0^2 - \omega^2 - i\gamma\omega} \right) \frac{\partial^2 \mathbf{E}}{\partial t^2} \quad (2.13)$$

where we have used the relation $1/c^2 = \mu_0\epsilon_0$ and μ_0 is the permeability of free space. Already we can see from equation (2.13) that the electric field

in such a medium is not only time dependent but is affected by a material property (terms in bracket). If we consider a plane wave of the form

$$\mathbf{E} = \mathbf{E}_0 e^{i(kz - \omega t)} \quad (2.14)$$

where k is the wave number. Using this as a trial solution for equation (2.13), then

$$-\nabla^2 \mathbf{E} = -k^2 \mathbf{E} \quad (2.15)$$

and

$$\frac{\partial^2 \mathbf{E}}{\partial t^2} = -\omega^2 \mathbf{E}. \quad (2.16)$$

Substituting equations (2.15) and (2.16) into the wave equation (2.13) gives an expression for k which is the wave number and relates to the behavior of the light in the medium as

$$k^2 = \frac{\omega^2}{c^2} \left(1 + \frac{Ne^2}{m\epsilon_0} \cdot \frac{1}{\omega_0^2 - \omega^2 - i\gamma\omega} \right). \quad (2.17)$$

The imaginary term in the denominator of the expression above means that the wave number k must be a complex number having a real and imaginary part, meaning that we can write k in terms of its real and imaginary parts as

$$k = k_R + ik_i \quad (2.18)$$

Since the wave number is related to the refractive index by the factor $\frac{\omega}{c}$, where ω is the angular frequency of the wave and c is the speed of light. We can also write the refractive index η in terms of its real and imaginary parts as

$$\eta = \eta_R + i\eta_i \quad (2.19)$$

With equation (2.18) we can rewrite our solution based on equation (2.14) as

$$\mathbf{E} = \mathbf{E}_0 e^{-k_i z} e^{i(k_R z - \omega t)} \quad (2.20)$$

The factor $e^{-k_i z}$ shows that the amplitude of the wave decreases as it propa-

gates through the medium, this is as a result of the absorption of the energy of the wave by the medium. This absorption is very large at resonant frequencies. Since the intensity of the wave is given by the square of the magnitude of the electric field, the absorption coefficient $\alpha = 2k_i$. Using equation (2.17) and (2.19), and equating the real and imaginary parts of the refractive index, we get

$$\eta_i^2 - \eta_R^2 = 1 + \frac{Ne^2}{m\epsilon_0} \left(\frac{\omega_0^2 - \omega^2}{(\omega_0^2 - \omega^2) - \gamma^2\omega^2} \right) \quad (2.21)$$

and

$$2\eta_i\eta_R = \frac{Ne^2}{m\epsilon_0} \left(\frac{\gamma\omega}{(\omega_0^2 - \omega^2) - \gamma^2\omega^2} \right) \quad (2.22)$$

The interesting parameters $\eta_R(\omega)$ and $\eta_i(\omega)$ which denotes the frequency dependent refractive index (dispersion) of the material and absorption of light by the material respectively are obtained using equation(2.21) and (2.22). Figures (2.1) and (2.2) shows how these parameters behave and we can make the following deductions.

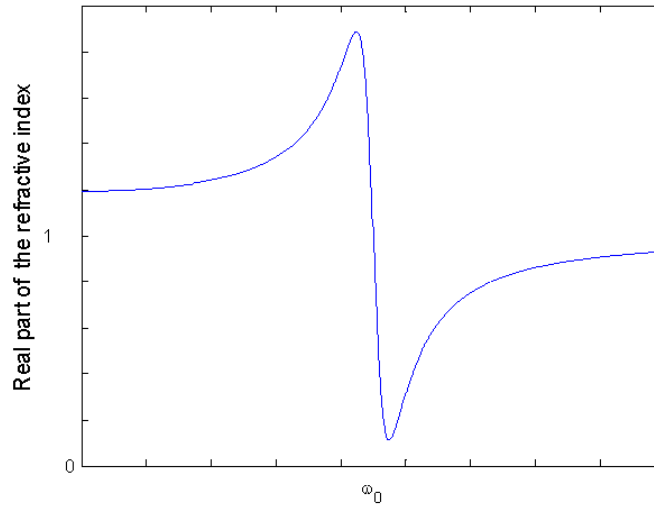


Figure 2.1: Real part of the refractive index versus frequency

The index of refraction is slightly greater than 1 for small frequencies and increases rapidly with frequency as it approaches the resonant frequency. This is the “normally dispersive” region, for most transparent media this

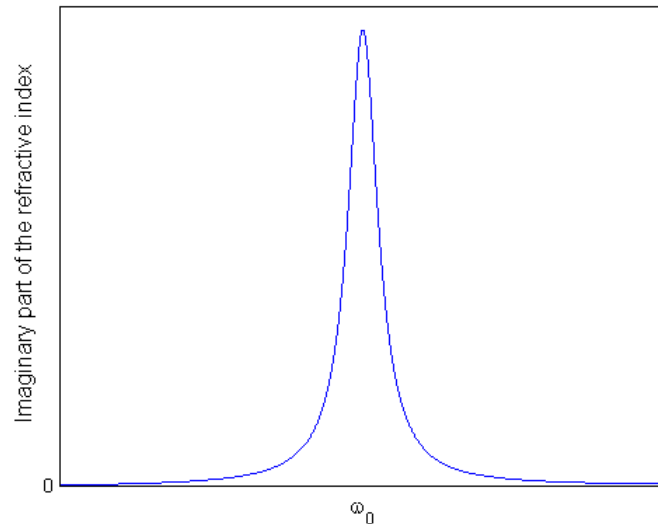


Figure 2.2: Imaginary part of the refractive index versus frequency

covers the visible spectral region. On the other hand anomalous dispersion involves a decrease in the refractive index with increasing frequency.

2.3 Optical dispersion in materials

From the previous section we have understood that the refractive index of a material increases with frequency in normally dispersive media and this effect is termed dispersion. As a result of the wide spectral width of ultrashort optical pulses, and group velocity dispersion (GVD) in transparent media, dispersion is usually of interest in ultrashort optics. The propagation of the different spectral components in the pulse spectrum results in a spatial and temporal broadening of the pulse. In materials with positive group velocity dispersion, that is, normally dispersive media, the longer wavelengths travel faster than the shorter ones, and in anomalous dispersive regions the reverse is the case (see figure 2.1). Figure (2.3) shows the dispersion curve for fused silica illustrating an increase in refractive index with wavelength.

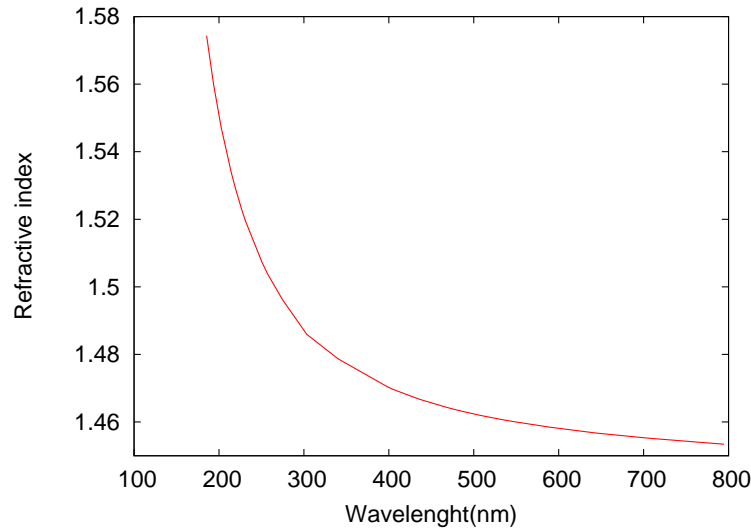


Figure 2.3: Dispersion curve for fused quartz

2.4 Ultrashort pulse propagation in a dispersive medium

A short pulse propagating through a medium such as an optical dispersive material, might become distorted in shape or broadened in time depending on the specific material and on the distance z along the direction of propagation. In this section we try to analyze this phenomena.

In practice, an ultrashort pulse is polychromatic that is, it consist of many frequency components within the visible region of the electromagnetic spectrum. Ideally the instantaneous frequency of the pulse should be constant in time. In such a situation the pulse is said to be transform limited. However if a broad spectral width pulse enters a dispersive medium, the different frequency components experiences different values of the refractive index, this means they each travel at slightly different speeds. The result of this phenomena is an increase in the duration of the pulse, the pulse is thus said to be *chirped*. Now we want to analyze this phenomena in relation to an ultrashort pulse. Assuming a Gaussian envelope for the electric field of the form

$$E(t, 0) = \exp(-a_0 t^2 + i\omega_0 t), \quad (2.23)$$

implies an electric field in the frequency domain given by [18]

$$E(0, \omega) = \exp\left[-\frac{(\omega - \omega_0)^2}{4a_0}\right] \quad (2.24)$$

By choosing the pulse in the form described in (2.23) note that we have considered initially an unchirped pulse with pulse parameter $a_0 = a - ib$ with $b = 0$. The output pulse spectrum after propagating a distance z through a dispersive medium will be the initial spectrum as expressed in (2.24), multiplied by the frequency-dependent propagation through the system (we have already established this in section (2.1)). This gives

$$E(z, \omega) = E(\omega, 0) \exp(-ik(\omega)z) \quad (2.25)$$

where $k(\omega) = \eta(\omega)\omega/c$ is the wave number of the dispersive medium, $\eta(\omega)$ is the refractive index corresponding to a particular frequency component or wavelength and c is the speed of light in vacuum. Considering cases of relatively narrow band signals having frequency components around some center frequency ω_0 , then the propagation constant can be expanded about its value at ω_0 in the form [18]

$$k(\omega) = k(\omega_0) + k'(\omega - \omega_0) + \frac{1}{2}k''(\omega - \omega_0)^2 \quad (2.26)$$

where the derivatives $k' = dk/d\omega$ and $k'' = d^2k/d\omega^2$ are evaluated at $(\omega - \omega_0)^2$. Then $E(z, \omega)$ can be expressed as [18]

$$E(z, \omega) = \exp\left[-ik(\omega_0)z - ik'z(\omega - \omega_0) - \left(\frac{1}{4a_0} + \frac{ik''z}{2}\right)(\omega - \omega_0)^2\right] \quad (2.27)$$

The output pulse in time domain after a distance z will then be the inverse Fourier transform of the output spectrum, that is

$$\begin{aligned} E(z, t) &\equiv \int_{-\infty}^{\infty} E(z, \omega) \exp(i\omega t) d(\omega - \omega_0) \\ &= \int_{-\infty}^{\infty} \exp \left[-ik(\omega_0)z - ik'z(\omega - \omega_0) - \left(\frac{1}{4a_0} + \frac{ik''z}{2} \right) (\omega - \omega_0)^2 \right] \exp(i\omega t) d(\omega - \omega_0) \end{aligned} \quad (2.28)$$

The integral in equation (2.28) can be rewritten in the form (see appendix A.1)

$$E(z, t) = \frac{e^i [\omega_0 t - k(\omega_0)z]}{2\pi} \int_{-\infty}^{\infty} \exp \left[-\frac{(\omega - \omega_0)^2}{4a(z)} + i(\omega - \omega_0)(t - k'z) \right] d(\omega - \omega_0) \quad (2.29)$$

where $1/a(z) \equiv 1/a_0 + 2ik''$. The advantage of rearranging in this form is that the carrier-frequency time and space dependence have been moved out of the integral, so that the integrand of the expression gives the time and space dependence of the output pulse envelope. From equation (2.29) we can see that the output pulse is still a Gaussian pulse but with an altered Gaussian pulse parameter $a(z)$. In order to interpret this mathematical result, we can carry out the integration using ‘‘Siegman’s lemma,’’ given by [18]

$$\int_{-\infty}^{\infty} e^{Ay^2 - 2By} dy \equiv \sqrt{\frac{\pi}{A}} e^{B^2/A}, \quad \text{Re}[A] > 0 \quad (2.30)$$

or we can note that the integrand of equation (2.29) is the Fourier transform of a Gaussian pulse in the form $\exp(-at^2)$, with a shift in time by $t - k'z$. These two approaches give the output pulse after traveling a distance z through the medium as

$$\begin{aligned} E(z, t) &= \exp [i(\omega_0 t - k(\omega_0)z)] \exp \left[-a(z) (t - k'z)^2 \right] \\ &= \exp \left[i\omega_0 \left(t - \frac{z}{v_\phi(\omega_0)} \right) \right] \exp \left[-a(z) \left(t - \frac{z}{v_g(\omega_0)} \right)^2 \right] \end{aligned} \quad (2.31)$$

where $a(z)$ is the modified Gaussian pulse parameter after traveling a distance z . This term is usually smaller than the initial parameter a_0 showing that the pulse width has been broadened. Some interpretations can now be made from the expression for $E(z, t)$ given in equation (2.31). From the first exponential term it is seen that the phase of the carrier frequency is delayed by a phase shift $k(\omega_0)z$ or a midband phase delay in time t_ϕ given by

$$t_\phi = \frac{z}{v_\phi(\omega_0)} = \frac{k(\omega_0)}{\omega_0}z. \quad (2.32)$$

This means that the sinusoidal waves within the pulse envelope will seem to move forward with a phase velocity of

$$v_\phi(\omega_0) = \frac{z}{t_\phi} = \frac{\omega_0}{k(\omega_0)} \quad (2.33)$$

The phase velocity is determined by the propagation $k(\omega_0)$ at the carrier frequency ω_0 .

The second exponent in (2.31) shows that the pulse envelope remains a Gaussian but with a modified pulse parameter $a(z)$, and is delayed by the group delay time t_g given by

$$t_g = \frac{z}{v_g(\omega_0)} = k'z. \quad (2.34)$$

This means the pulse envelope appears to move forward with a group velocity

$$v_g(\omega_0) = \frac{1}{(dk/d\omega)} = \left(\frac{d\omega}{dk} \right). \quad (2.35)$$

To summarize this discussion, we showed that an ultrashort pulse propagating through a lossless (ignoring absorption) homogeneous media will experience a delay of the pulse, and an increase in duration due to a frequency chirp.

3. Description of an ultrashort pulse

3.1 Temporal and spectral representations

The fundamental quantity describing an individual pulse of light is the real electric field which is a function of time and space or frequency and wave vector. Consider again a Gaussian pulse shape, and rewrite equation (2.23) and equation (2.24). The Gaussian pulse time domain electric field with constant phase (figure 3.1) can be written as

$$E(t) = \exp(-at^2 + i\omega_0 t) \quad (3.1)$$

where a is proportional to the inverse of the square of the pulse duration, that is $a \propto 1/t_p^2$. Equation (3.1) describes a pulse that has a constant instantaneous frequency in time. The time dependent intensity of the pulse $|E(t)|^2$ can be measured and for a constant phase can be represented as in figure (3.1)

The Fourier transform of equation (3.1) gives the frequency representation of the light pulse as

$$E(\omega) = \exp\left[-\frac{(\omega - \omega_0)^2}{4a}\right] \quad (3.2)$$

and the width of the spectrum is directly proportional to a . We can see that there is a relationship between the spectral width of the pulse and the pulse duration. The exact relationship between these quantities will be shown in the next section.

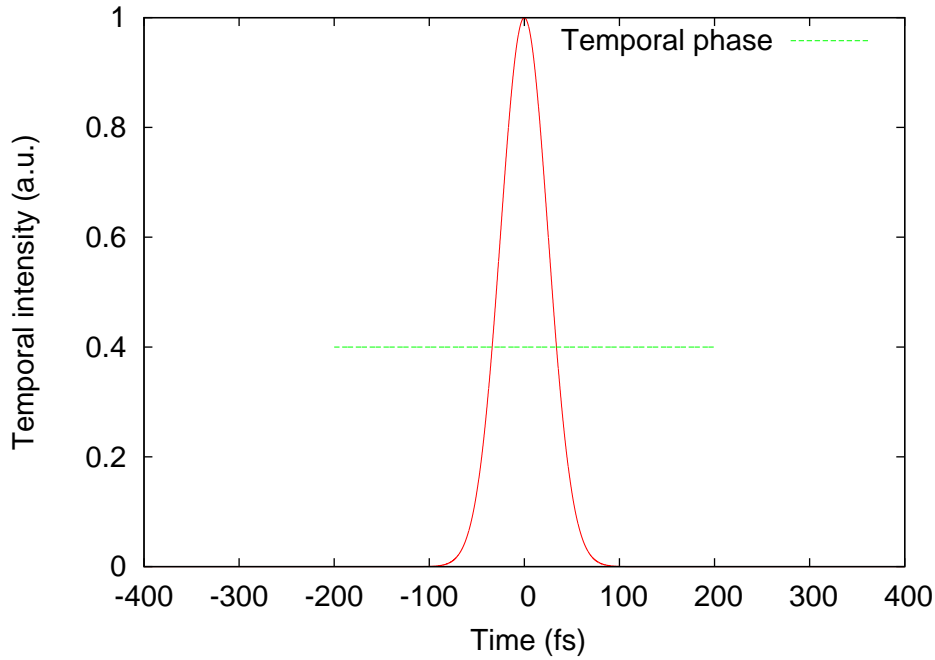


Figure 3.1: Temporal intensity of a Gaussian pulse with constant phase

3.2 Time bandwidth product

In general the time-frequency relationship of a light pulse can be represented as

$$E(t) = \frac{1}{2\pi} \int_{-\infty}^{\infty} E(\omega) e^{-i\omega t} d\omega \quad (3.3)$$

and

$$E(\omega) = \int_{-\infty}^{\infty} E(t) e^{i\omega t} dt \quad (3.4)$$

The duration and spectral width of the pulse are usually calculated using standard statistical definitions [3]

$$\begin{aligned} \langle \Delta t \rangle &= \frac{\int_{-\infty}^{\infty} t |\varepsilon(t)|^2 dt}{\int_{-\infty}^{\infty} |\varepsilon(t)|^2 dt}, \\ \langle \Delta \omega^2 \rangle &= \frac{\int_{-\infty}^{\infty} \omega^2 |E(\omega)|^2 d\omega}{\int_{-\infty}^{\infty} |E(\omega)|^2 d\omega}. \end{aligned} \quad (3.5)$$

The spectral width and pulse duration can be shown to be related by the quantities

$$\Delta\omega\Delta t \geq \frac{1}{2} \quad (3.6)$$

So we note that a short pulse duration Δt requires a large frequency range $\Delta\omega$ to describe the pulse. In order to generate an ultrashort pulse, it is therefore necessary that the laser is characterized with a large gain bandwidth and a large number of longitudinal modes. Equation (3.6) also shows that there is a limit to the time-bandwidth product. The idea of a theoretical limit to the time-bandwidth product of a pulse can be explained better using Fourier transformations. Considering the case of the Gaussian pulse envelope. The Full Width at Half Maximum (FWHM) of the temporal intensity profile is given by

$$\Delta t = \sqrt{\frac{2\ln(2)}{a}} \quad (3.7)$$

and the FWHM of the spectrum is

$$\Delta\nu = \frac{\Delta\omega}{2\pi} = \sqrt{\frac{2\ln(2)a}{\pi}} \quad (3.8)$$

The time-bandwidth product is then

$$\Delta\nu\Delta t = \frac{2\ln(2)}{\pi} = 0.441 \quad (3.9)$$

Equation (3.9) gives a theoretical minimum for the time-bandwidth product of the pulse. This value depends on the assumed pulse shape (see table 3.1) and holds for pulses without frequency modulation or unchirped pulses. We defined the term “chirped pulse” in the previous section. A pulse whose time-bandwidth product is given by the theoretical minimum is called a “Fourier-limited” or “bandwidth limited” pulse. The electric field of a bandwidth limited Gaussian pulse will be of the form given in figure 3.2

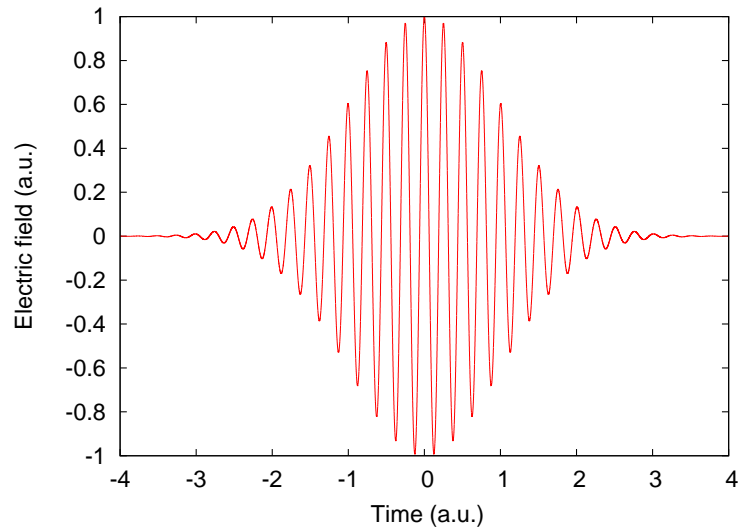


Figure 3.2: Bandwidth limited Gaussian pulse

and is characterized by a constant frequency with time. In reality, due to inevitable chirp a pulse bandwidth product will be greater than the theoretical minimum. For some applications it is important that the pulse is close to the transform limit.

Shape	$E(t)$	$C = \Delta\nu\Delta t$
Gaussian function	$\exp(-at^2)$	0.441
Exponential function	$\exp(-at)$	0.140
Lorentzian Pulse	$[1 + (at)^2]$	0.142
Hyperbolic secant	$\frac{1}{\cosh(at)}$	0.315
Cardinal sine	$\frac{\sin^2(at)}{at^2}$	0.336
Rectangle	—	0.892

Table 3.1: Values of time-bandwidth constants C for selected pulse shapes

3.3 Variation of instantaneous frequency with time

As was mentioned earlier, in reality, the time-bandwidth product of the pulse will not usually be given by the theoretical minimum, that is, the pulse will

originally not be bandwidth limited. This is due to the effects of dispersion and nonlinearities. A pulse that is not bandwidth limited is said to be a chirped pulse. A chirped pulse is one whose instantaneous frequency varies during the duration of the pulse. A brief mathematical description of a chirped pulse is given below. This will help us understand the complexities of chirp in a pulse. The time-varying phase-shift or phase rotation of the sinusoidal signal within this Gaussian pulse is given by

$$E(t) \propto \exp[i(\omega_0 t + \phi(t))] \quad (3.10)$$

where the temporal phase $\phi(t)$ contains the frequency versus time information. For a start we assume

$$\phi(t) = \beta t^2 \quad (3.11)$$

as a first approximation. We will explain shortly what the parameter β describes. The signal can then be expressed as

$$E(t) \propto \exp[i(\omega_0 t + \beta t^2)] \quad (3.12)$$

The total instantaneous phase of the signal denoted by ϕ_o is given by

$$\phi_o(t) = \omega_0 t + \beta t^2 \quad (3.13)$$

The instantaneous angular frequency is defined as the rate at which the total phase of the sinusoidal signal rotates forward, this can be expressed as

$$\omega_{inst}(t) \equiv \frac{d\phi_o(t)}{dt}. \quad (3.14)$$

Considering the complex Gaussian with instantaneous angular frequency given by

$$\omega_{inst}(t) \equiv \frac{d}{dt}(\omega_0 t + \beta t^2) = \omega_0 + 2\beta t. \quad (3.15)$$

The complexity of the phase of the signal determines the complexity of the frequency versus time variation. A Gaussian pulse with a non-zero imaginary part β , therefore has a linearly time-varying instantaneous frequency. Such

a signal is said to be chirped, with the parameter β being a measure of this chirp. In the case we illustrated above, we have been considering pulses whose instantaneous frequency increases linearly with time, this is called a positively chirped pulse. On the other hand, if the instantaneous frequency decreases with time we get a negatively chirped Gaussian pulse. We simply make β negative.

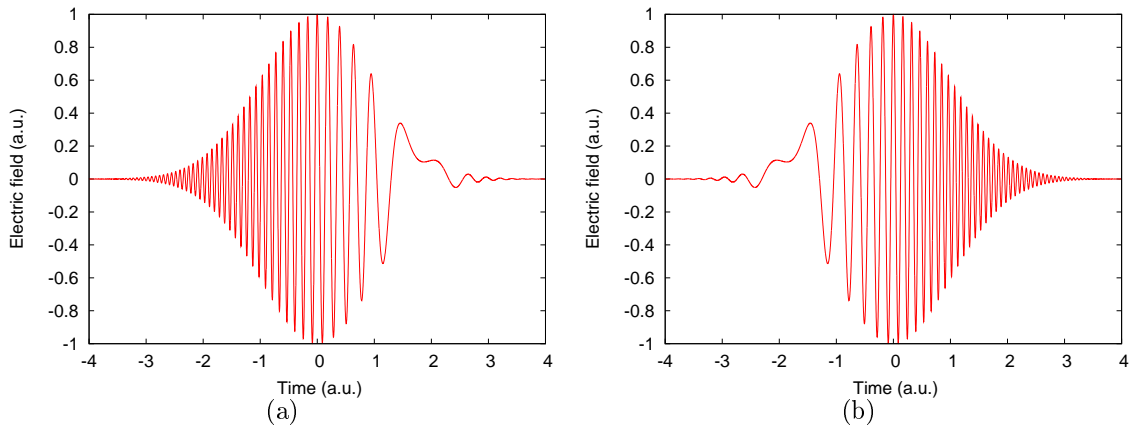


Figure 3.3: (a) Negatively chirped Gaussian pulse (b) Positively chirped Gaussian pulse

The frequency of the light wave can also vary nonlinearly with time. Consider the case where it varies quadratically with time

$$\omega_{inst} = \omega_0 + 3\gamma t^2 \quad (3.16)$$

where γ is a measure of the quadratic chirp. The phase of field is given by

$$E(t) \propto \exp[i(\omega_0 t + \gamma t^3)] \quad (3.17)$$

Dispersion has played an important role in ultrafast laser physics. A typical example is in the *chirped pulse amplification* system (CPA) which is the main component in ultrashort pulse amplifiers. CPA requires proper dispersion management to produce ultrashort, high energy pulses [19]. In this system the short pulse to be amplified is first stretched temporarily, by passing it

through a dispersive delay line typically one with a positive group delay dispersion. This reduces the peak intensity and the pulse is now safely amplified by several passes through a broad band gain medium. After amplification the pulse is recompressed in a dispersive delay line, with opposite sign to that of the stretcher. The compressor “corrects” the dispersion induced by the gain medium, resulting in an ultrashort high energy pulse. See figure 3.4.

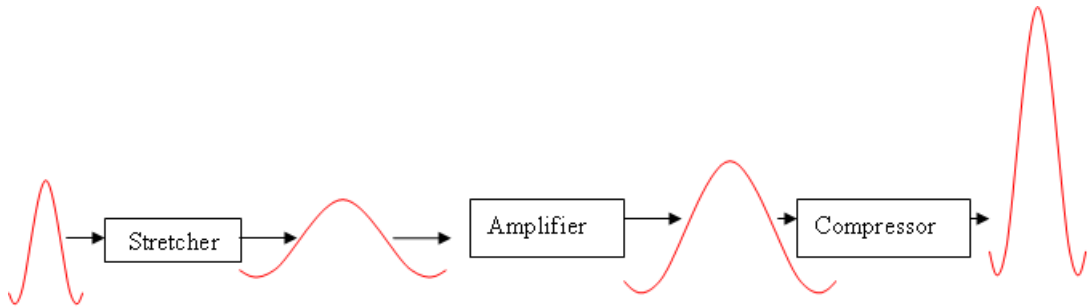


Figure 3.4: Illustration of the principle of chirped pulse amplification technique

4. Nonlinear optical processes

The nonlinear optical effect has been a useful tool in the characterization of ultrashort pulses. It is interesting to note that while there exist a problem of ultrashort pulse characterization due to the very short duration of these pulses, the high intensities of these pulses allow for the use of nonlinear optical process to characterize the pulse profile either in the temporal or spatial domain. Nonlinear optical processes became measureable after the demonstration of the ruby laser by Theodore Harold Maiman in July, 1960. It was however first implemented by Franken and his colleagues in 1961 [20]. A 694.3 nm light from a ruby laser was focused into a quartz crystal and a very low energy beam of wavelength 347.15 nm was detected. Though with a poor conversion efficiency, the demonstration of this experiment brought great enthusiasm and opened a new world for significant nonlinear optical interactions. Preceding this time, the polarization of a material was assumed to be linear with the induced electric field \mathbf{E}

$$\mathbf{P} = \epsilon_0 \chi \mathbf{E} \quad (4.1)$$

where ϵ_0 is the permittivity of free space and χ is the linear susceptibility which is a property of the material. However, if the applied electric field is high enough as in the case of lasers, the nonlinear terms in the polarization of a material can no longer be ignored. The nonlinear polarization can then be described as a power series expansion of the electric field [2]

$$P_{NL} = \epsilon_0 (\chi^{(1)} E + \chi^{(2)} E^2 + \dots) \quad (4.2)$$

Here $\chi^{(2)}$ is the second order non-linear susceptibility of the material and the nonlinear polarizability P_{NL} is seen to depend nonlinearly on the fundamental applied field. In centrosymmetric materials the even terms vanish. Assuming a linear relationship between the polarization of a material and the input electric field implies that the intensity of the applied field is small enough to ignore the higher order contributions of the field to the polarization of the

material. Nonlinear optical processes have found a variety of applications in ultrashort laser studies and of interest to this project is its application in optical short pulse characterization. Most self-referencing techniques used for pulse characterization require a nonlinear interaction of the test pulse in a medium. Second harmonic generation which relates to the second term in the nonlinear polarization is often utilized.

4.1 The origin of nonlinear polarization

In section 2.2 we had modelled the linear response of the electrons in a medium using the electron oscillator model. Similarly in this section we will model the nonlinear atomic response of a noncentrosymmetric medium, (mediums lacking inversion symmetry) by allowing for nonlinearity in the restoring force exerted on the electrons. In this case, the restoring force on the electrons is not limited to Hooke's law

$$\mathbf{F} = -K\mathbf{r}$$

but higher order terms become significant (larger), considering only the first two terms

$$\mathbf{F} = -K_1\mathbf{r} - K_2\mathbf{r}^2 + \dots$$

and we have neglected higher order terms. The Equation of motion of an electron then becomes [2]

$$\ddot{\mathbf{r}} + \gamma\dot{\mathbf{r}} + \omega_0^2\mathbf{r} + \mathbf{r} \cdot \tilde{a} \cdot \mathbf{r} = -e\mathbf{E}(t)/m \quad (4.3)$$

where we have introduced a quadratic term, $\mathbf{r} \cdot \tilde{a} \cdot \mathbf{r}$, \tilde{a} being a third-rank tensor. For the sake of simplicity we will only consider the one dimensional case so that equation (4.3) can now be written as

$$\ddot{r} + \gamma\dot{r} + \omega_0^2r + ar^2 = -eE(t)/m. \quad (4.4)$$

We obtain this form by assuming that the restoring force is a nonlinear function of the displacement of the electron. Considering only the first and second term of the nonlinear expansion of the restoring force, we can understand the nature of the force by noting that it corresponds to a potential energy function of the form

$$U = - \int F dr = \frac{1}{2} m \omega_0^2 r^2 + \frac{1}{3} m a r^3 \quad (4.5)$$

Here the first term corresponds to a harmonic potential and the second term corresponds to an anharmonic correction term. This model corresponds to the physical situation of electrons in real materials, because the actual potential well that the atomic electron feels is not perfectly parabolic [2].

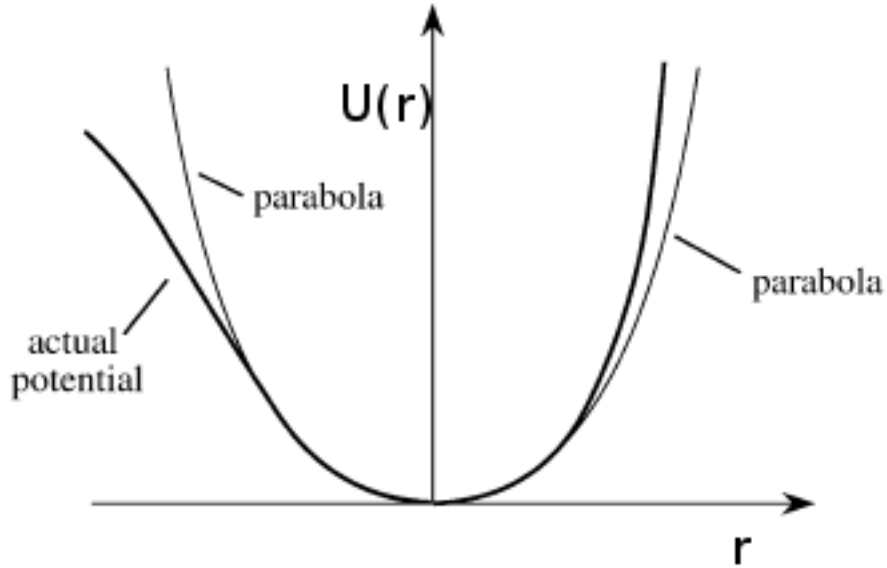


Figure 4.1: Potential energy function for a nonlinear medium [2]

In this case, let us assume that the applied optical field is of the form

$$E(t) = E_1 e^{i\omega_1 t} + E_2 e^{i\omega_2 t} + c.c..$$

No general analytic solution to equation (4.4) exist. However, if the applied

field is sufficiently weak, the nonlinear term ar^2 will be much smaller than the linear term $\omega_0^2 r$ for any displacement r . In order to solve equation (4.4) we use the idea of perturbation expansion [2]. This means we now replace $E(t)$ by $\lambda E(t)$, where λ is a parameter that ranges continuously between zero and one. The expansion parameter λ thus characterizes the strength of the perturbation. Equation (4.4) then becomes

$$\ddot{r} + \gamma\dot{r} + \omega_0^2 r + ar^2 = -\lambda eE(t)/m \quad (4.6)$$

Note here that λ in this Section has nothing to do with wavelength, and we just employ this method because we need to solve the equation (4.4).

We now seek a solution to Equation (4.6) in the form of a power series expansion, that is

$$r = \lambda r^{(1)} + \lambda^2 r^{(2)} + \lambda^3 r^{(3)} + \dots \quad (4.7)$$

Using only the first and second term, substituting into equation (4.6), and equating the coefficients of the first and second powers of λ , we obtain the following equations for the coefficients of λ^1 and λ^2 respectively as

$$\ddot{r}^{(1)} + \gamma\dot{r}^{(1)} + \omega_0^2 r^{(1)} = -eE(t)/m \quad (4.8)$$

$$\ddot{r}^{(2)} + \gamma\dot{r}^{(2)} + \omega_0^2 r^{(2)} + a[r^{(1)}]^2 = 0 \quad (4.9)$$

Notice that equation (4.8) is the same as the equation of motion describing the linear response of the atoms to the electric field we obtained in equation (2.9), and we have already found the solution in equation (2.11). In order to solve equation (4.9), we choose a solution of the form

$$r^{(1)}(t) = r^{(1)}(\omega_1)e^{-i\omega_1 t} + r^{(1)}(\omega_2)e^{-i\omega_2 t} + c.c \quad (4.10)$$

where the amplitudes $r^{(1)}(\omega_j)$ have the form

$$r^{(1)}(\omega_j) = -\frac{e}{m} \frac{E_j}{D(\omega_j)} \quad (4.11)$$

and we introduce the complex denominator function

$$D(\omega) = \omega_0^2 - \omega^2 - i\omega\gamma. \quad (4.12)$$

Squaring equation (4.10) gives

$$\begin{aligned} [r^{(1)}(t)]^2 &= [r^{(1)}(\omega_1)]^2 e^{-2i\omega_1 t} + 2r^{(1)}(\omega_1)r^{(1)}(\omega_2)e^{-i(\omega_2+\omega_1)t} + [r^{(1)}(\omega_2)]^2 e^{-2i\omega_2 t} \\ &+ 2r^{(1)}(\omega_1)r^{(1)*}(\omega_2)e^{-i(\omega_1-\omega_2)t} + 2r^{(1)*}(\omega_1)r^{(1)}(\omega_2)e^{-i(\omega_2-\omega_1)t} \\ &+ 2r^{(1)*}(\omega_1)r^{(1)*}(\omega_2)e^{-i(-\omega_1-\omega_2)t} + [r^{(1)*}(\omega_1)]^2 e^{-i(-2\omega_1)t} + [r^{(1)*}(\omega_2)]^2 e^{-i(2\omega_2)t} \\ &+ 2r^{(1)}(\omega_1)r^{(1)*}(\omega_1) + 2r^{(1)}(\omega_2)r^{(1)*}(\omega_2) \end{aligned}$$

Notice that the square of $r^{(1)}(t)$ contains the frequencies $\pm 2\omega_1$, $\pm 2\omega_2$, $\pm(\omega_1 + \omega_2)$, $\pm(\omega_1 - \omega_2)$ and 0. We see here, and for the first time, the source of the second-order optical effects. When we considered the second order term in the nonlinear displacement of the electrons by the applied force, and solved the equation of motion for the electrons, we notice the second order nonlinear effects such as the frequency doubled beam ($2\omega_1$ and $2\omega_2$) and the sum frequency beam ($\omega_1 + \omega_2$). In order to determine the response of the material at frequency $2\omega_1$, for instance, we must solve the equation

$$\ddot{r}^{(2)} + \gamma\dot{r}^{(2)} + \omega_0^2 r^{(2)} = -a [r^{(1)}(\omega_1)]^2 \quad (4.13)$$

and this implies solving

$$\ddot{r}^{(2)} + \gamma\dot{r}^{(2)} + \omega_0^2 r^{(2)} = -a \left[\frac{e^2}{m^2} \frac{E_1^2 e^{-2i\omega_1 t}}{D^2(\omega_1)} \right] \quad (4.14)$$

We seek a solution of the form

$$r^{(2)}(t) = r^{(2)}(2\omega_1)e^{-i2\omega_1 t} \quad (4.15)$$

Substituting Equation (4.15) into Equation (4.14) we get that

$$(-4\omega_1^2 - 2i\gamma\omega_1 + \omega_0^2) r^{(2)}(2\omega_1)e^{-2i\omega_1 t} = -a \left[\frac{e^2}{m^2} \frac{E_1^2 e^{-2i\omega t}}{D^2(\omega_1)} \right] \quad (4.16)$$

and this implies

$$r^{(2)}(2\omega_1) = -a \left[\frac{e^2}{m^2} \frac{E_1^2}{D(2\omega_1)D^2(\omega_1)} \right] \quad (4.17)$$

where

$$D(2\omega_1) = -4\omega_1^2 - 2i\omega_1\gamma + \omega_0^2 \quad (4.18)$$

Similarly, the amplitudes of the response at frequency $2\omega_2$ is found to be

$$r^{(2)}(2\omega_2) = -a \left[\frac{e^2}{m^2} \frac{E_1^2}{D(2\omega_2)D^2(\omega_1)} \right] \quad (4.19)$$

The linear contribution to polarization from Equation (2.8) is given in a more general form by

$$P^{(1)}(\omega_1) = -Ner^{(1)}(\omega_j)$$

then using equation (4.11), we can now write $P^{(1)}(\omega_1)$ as

$$P^{(1)}(\omega_1) = \frac{Ne^2 E_j}{mD(\omega_j)} \quad (4.20)$$

From equation (4.20), we define the linear susceptibility in general as

$$\chi^{(1)}(\omega_i) = \frac{Ne^2}{mD(\omega_j)}$$

so that the linear polarization in a more general form is defined by

$$P^{(1)}(\omega_1) = \chi^{(1)}(\omega_j)E(\omega_i) \quad (4.21)$$

The nonlinear polarization and susceptibilities are calculated in an analogous manner. The nonlinear susceptibility describing second-harmonic generation

$\chi^{(2)}$ is defined by the relation

$$P^{(2)}(2\omega_1) = \chi^{(2)}(2\omega_1, \omega_1, \omega_1)E(\omega_1)^2 \quad (4.22)$$

Here ,

$$\chi^{(2)}(2\omega_1, \omega_1, \omega_1) = \frac{N(e^3/m^2)a}{D(2\omega_1)D^2(\omega_1)} \quad (4.23)$$

and $P^{(2)}(2\omega_1)$ is the nonlinear polarization source for the second-harmonic generation.

From equation (4.22), we see that the nonlinear polarization source for the second-harmonic generation depends on the square of the incident electric field. The invention of lasers with high intensity light brought to the fore the nonlinear optical effects in materials. Also, the nonlinear polarization source for the second-harmonic generation depends on the nonlinear susceptibility $\chi^{(2)}(2\omega_1, \omega_1, \omega_1)$ expressed in equation (4.23). In the denominator of this susceptibility, we see from equation (4.12) and (4.18), that the second order nonlinear susceptibility $\chi^{(2)}(2\omega_1, \omega_1, \omega_1)$ may be resonantly enhanced at the frequencies ($\omega_0 \approx \omega_1$ and $\omega_0 \approx 2\omega_1$). In resonant enhancement processes the frequency of the lasers is tuned, so that it is close to the resonant frequency of the material. This increases the susceptibility.

This section helps to understand that if we consider the application of an intense electric field to a medium, the expression for a linear polarization obtained in equation (4.1) does not describe the polarization of a medium completely. From the electron model we would say that the displacement r of the electrons is no longer small since the field is intense and so we must consider at least the quadratic term in the nonlinear expansion of the elastic restoring force. Doing this, we discovered that the polarization of a nonlinear medium is expressed as a power series in the applied electric field. Since the second order nonlinear processes, in particular second harmonic generation is mainly utilized in pulse characterization let us look briefly at these concept.

4.2 Second harmonic generation (SHG)

Second harmonic generation occurs when two photons of frequency ω are converted by a nonlinear process in a medium to a frequency of 2ω . Let us

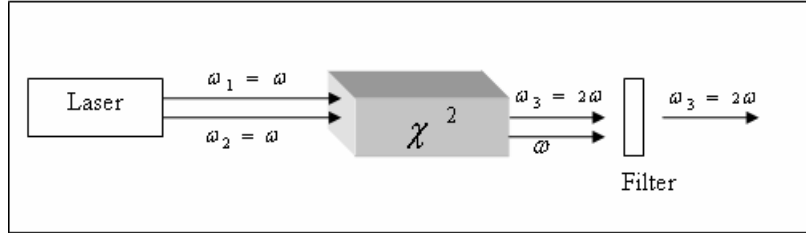


Figure 4.2: Schematic of the principle underlying second harmonic generation

consider the case in which two input photons have different frequencies ω_1 and ω_2 , and $\omega_1 \neq \omega_2$. The total incident electric field can be written as

$$E = E_1 e^{-i\omega_1 t} + E_1^* e^{i\omega_1 t} + E_2 e^{-i\omega_2 t} + E_2^* e^{i\omega_2 t} \quad (4.24)$$

The second order nonlinear polarizability from equation (4.2) is then

$$\begin{aligned} P^{(2)} &= \epsilon_0 \chi^{(2)} E^2 \\ &= \epsilon_0 \chi^{(2)} [E_1^2 e^{-i(2\omega_1)t} + (E_1^*)^2 e^{i(2\omega_1)t} + E_2^2 e^{-i(2\omega_2)t} + (E_2^*)^2 e^{i(2\omega_2)t} \\ &\quad + 2E_1 E_1^* + 2E_2 E_2^* + 2E_1 E_2 e^{-i(\omega_1 + \omega_2)t} + 2E_1^* E_2^* e^{i(\omega_1 + \omega_2)t} \\ &\quad + 2E_1 E_2^* e^{-i(\omega_1 - \omega_2)t} + 2E_1^* E_2 e^{i(\omega_1 - \omega_2)t}] \end{aligned}$$

Note that the induced second order polarization contains the second-harmonic terms with $2\omega_1$ and $2\omega_2$, the direct current terms representing a time independent factor that produces no oscillating electromagnetic radiation, the sum-frequency generation (SFG) corresponding to the addition of the two fundamental frequencies $\omega_1 + \omega_2$ and the difference frequency generation (DFG) $\omega_1 - \omega_2$. For efficient second harmonic generation, it is desirable that the nonlinear optical medium possess properties such as high optical power damage threshold, transparency over a large range of frequencies, large effective second order susceptibility (see appendix A.2) and it is essential that the

medium is a non-centrosymmetric medium. Symmetry constraints applies only to even order polarization of a material as they vanish in centrosymmetric materials. A centrosymmetric material is one whose structure remains unchanged upon inversion which implies replacing each coordinate \mathbf{r} with $-\mathbf{r}$ [20]. For such a material the electric field experiences the same polarization when the direction is reversed that is for the electric field \mathbf{E} , the polarization is

$$\mathbf{P}^{2n} = \epsilon_0 \sum_n \chi^{(2n)} \mathbf{E}^{2n} \quad (4.25)$$

and for a reverse direction $-\mathbf{E}$

$$-\mathbf{P}^{2n} = \epsilon_0 \sum_n \chi^{(2n)} (-\mathbf{E})^{2n} = \epsilon_0 \sum_n \chi^{(2n)} \mathbf{E}^{2n} \quad (4.26)$$

Since the contributions from \mathbf{E} and $-\mathbf{E}$ are the same, the total induced even order nonlinear polarization must be zero ($\chi^{(2n)} = 0$). Another very important condition necessary for second harmonic generation is phase matching.

4.3 Phase matching

Even when the other criteria necessary for second harmonic generation have been satisfied, there is still a need for phase matching. Phase matching in simple terms involves getting the fundamental wave and the second harmonic waves to be in phase. This implies traveling at the same speeds in the medium if the beams are collinear. This is especially critical when the length of the medium exceeds the coherence length. The coherence length is a certain fraction of the length L of the medium over which there is significant second harmonic generation and is usually very small, typically in the order of 10 μm [1]. The fundamental wave induces a nonlinear linear polarization that will normally travel slower than the fundamental wave through the length of the medium, due to normal dispersion. In this case, the efficiency of the second harmonic wave reduces again through the second coherence length in the medium because of constructive interference. The second harmonic

wave thus oscillates between a maximum intensity and zero intensity. Phase matching in crystals is typically achieved by using anisotropic birefringent materials which offer electromagnetic waves different refractive indices for different polarization directions in the material.

Generally the efficiency of the second harmonic wave depends on (see appendix A.2, equation (A.36))

$$C_{SHG} = \frac{I_{2\omega}(L)}{I_{\omega}(0)} \quad (4.27)$$

$$= 2 \left(\frac{\mu_0}{\epsilon_0} \right)^{3/2} \frac{\omega^2 d^2}{\eta^2(\omega)\eta(2\omega)} I_{\omega}(0) L^2 \left(\frac{\sin \frac{1}{2} \Delta k L}{\frac{1}{2} \Delta k L} \right)^2 \quad (4.28)$$

We can see that the efficiency of the second harmonic wave depends on the nonlinear susceptibility tensor, the intensity of the fundamental beam and the square of the total length of the crystal if phase matching has been achieved. To maximize this efficiency, phase matching is targetted at making Δk which corresponds to the difference in the refractive indices of the fundamental and second harmonic beam almost equal to zero. The phase matching factor for second harmonic wave is quantitatively given by the function

$$F(L_c) = \left(\frac{\sin \frac{1}{2} \Delta k L}{\frac{1}{2} \Delta k L} \right)^2 \quad (4.29)$$

This phase matching factor drops to about 40 percent after the “distance”

$$\frac{1}{2} \Delta k L = \frac{\pi}{2}$$

This leads to the definition of the coherence length as

$$L_c = \left| \frac{\pi}{\Delta k} \right|$$

From the expression for the conversion efficiency of the SHG in appendix A.2, (equation (A.36)) it can be seen that increasing the length of the crystal without phase matching does not improve the efficiency of the second

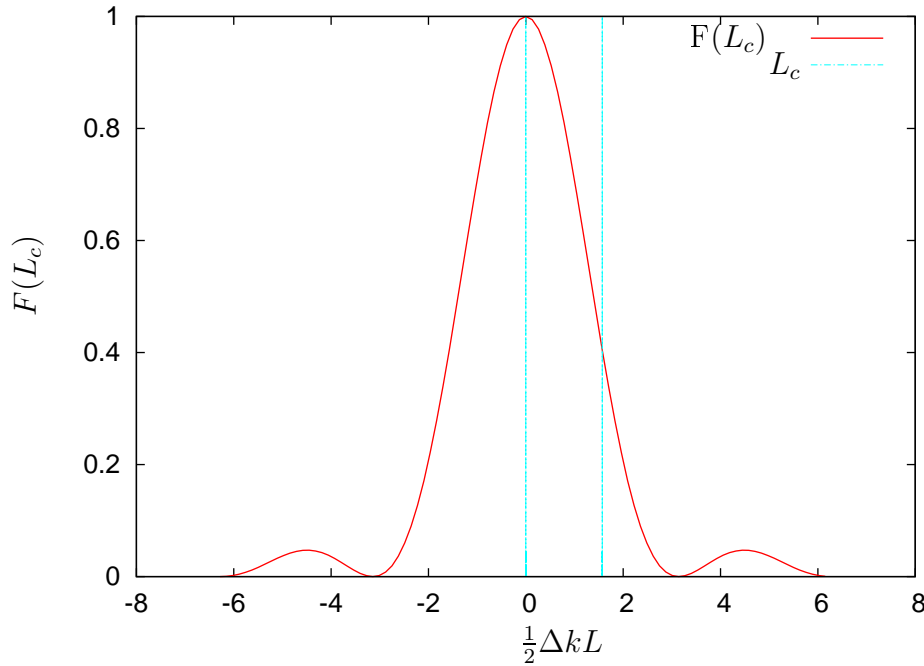


Figure 4.3: Phase matching factor of the conversion efficiency for the second harmonic wave

harmonic generated. However, increasing the coherence length does increase the efficiency [21]. The method of phase matching described above holds for the collinear geometry where the individual input photons having different or the same frequency propagates in the same direction. However, the individual photons can propagate in different directions and when such a geometry is utilized for phase matching it is referred to as non-collinear phase matching. Both collinear and non-collinear phase matching utilizes the principle of conservation of energy and conservation of momentum. The SPIDER experimental set up described in chapter 7 of this projects implements a noncollinear phase matching geometry for sum frequency generation. One advantage of the noncollinear geometry over the collinear one, is that it allows easy separation between the individual input photons and their second harmonics from the sum frequency beam as a result of the sum of the two input photons. Figure (4.4) shows how the beams emerging from the doubling crystal using non-collinear geometry are separated spatially [3]. Two beams with angular frequency ω and momenta \mathbf{k}_1 and \mathbf{k}_2 are incident on the

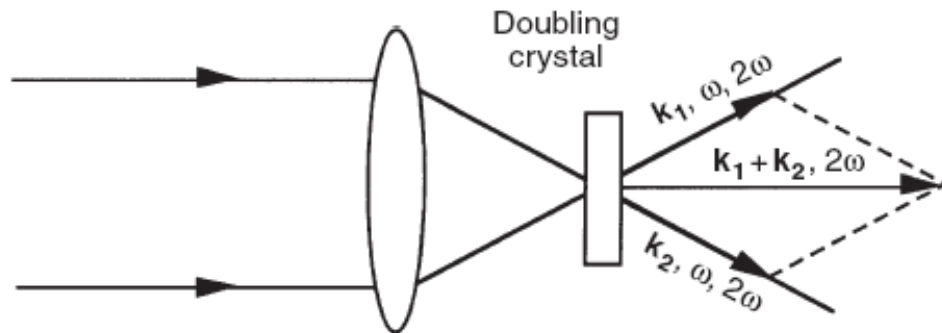


Figure 4.4: Non-collinear geometry for phase matching, energy and momentum is conserved

nonlinear crystal at an angle say β and produce one photon with angular frequency ω_2 and momentum \mathbf{k} . Energy conservation gives $\omega_2 = 2\omega$, and momentum conservation requires $\mathbf{k} = \mathbf{k}_1 + \mathbf{k}_2$, $\mathbf{k} = 2\mathbf{k}_1$, or $\mathbf{k} = 2\mathbf{k}_2$. For such a configuration in figure (4.4), five beams exit the crystal, two of them are at the fundamental frequency ω and in the directions \mathbf{k}_1 and \mathbf{k}_2 of the incident rays. Another two of the rays are the doubled beams of frequency 2ω and momentum vectors $2\mathbf{k}_1$ and \mathbf{k}_2 . The last beam of frequency 2ω propagates along the bisector of the angle β and the momentum from the geometry is $\mathbf{k}_1 + \mathbf{k}_2$.

5. Correlation techniques for ultrashort pulse characterization

In section 1.1 of this project, we gave motivations of why ultrashort pulse characterization is necessary. Unfortunately photoelectric response times are very slow and therefore limited when dealing with femtosecond laser pulses. For laser optimization and other significant reasons including those outlined in section 1.1 one wants to at least measure the pulse duration of femtosecond laser pulses and indirect techniques have to be used. Since these techniques are indirect, it is important to understand not only how the technique works, but also the model implemented to retrieve the desired information from the experimental data. Typically correlation techniques have been useful for measuring pulse duration of ultrashort pulses. Given two time-dependent functions, the probe pulse $g(t)$ and the test pulse $f(t)$, where $g(t)$ is known. The measurement of the cross correlation function [22]

$$G(t) = \int_{-\infty}^{\infty} g(t)f(t - \tau)dt \quad (5.1)$$

gives the test function $f(t)$. Higher order cross correlation functions can also be defined. The limitation of using the cross correlation measurement is that the probe or known pulse has to be shorter in time than the test pulse. Even when a temporally shorter pulse is available, like all correlation methods, the cross correlation function does not provide any information on the phase content of the test pulse [23]. Self referencing diagnostic techniques, where the unknown pulse is correlated with itself has been successfully implemented for measuring pulse durations and chirp parameters of short optical pulses. This is termed *autocorrelation* and practically involves delaying a copy of the test pulse with itself and measuring the correlation signal. Two main techniques used to implement autocorrelation measurements are the intensity autocorrelation and the interferometric autocorrelation techniques.

5.1 Intensity autocorrelation

The intensity autocorrelator uses a Michelson interferometer arrangement (figure (5.1)). The input beam is split into two and one of them undergoes a variable delay. The beams are recombined and directed into a nonlinear crystal for frequency doubling. A spatial filter is used to reject the unconverted fundamental beams as well as any second harmonic that is collinear to the fundamental beams which is detected by a photodiode. A signal can only be detected if the two pulses overlap in time since the intensity of the light generated by second harmonic generation scales as

$$I_{SHG} \propto I(t)I(t - \tau) \quad (5.2)$$

and is maximum at $\tau = 0$. Since the processes that occur in time t are much faster than the response time of the detector what is recorded is actually the intensity autocorrelation function given by [22]

$$G^2(\tau) = \frac{1 + \int_{-\infty}^{\infty} I(t)I(t - \tau)dt}{\int_{-\infty}^{\infty} I(t)^2dt} \quad (5.3)$$

A simulated intensity autocorrelation function assuming a Gaussian shaped pulse is shown in figure 5.2. The width of the autocorrelation function is related to the input pulse width, and depending on the shape assumed, the pulse width can be extracted from the autocorrelation signal (see Table 5.1). The intensity autocorrelation cannot provide information about the exact pulse shape due to the symmetric nature of the autocorrelation trace. Also because the pulse is used to measure it self, the intensity autocorrelation cannot provide information about the temporal or spectral phase of the pulse and information about the evolution of the pulse profile is lost. Another drawback of the intensity autocorrelation is that there exist pulses with different characteristics but having the same autocorrelation signal [22].

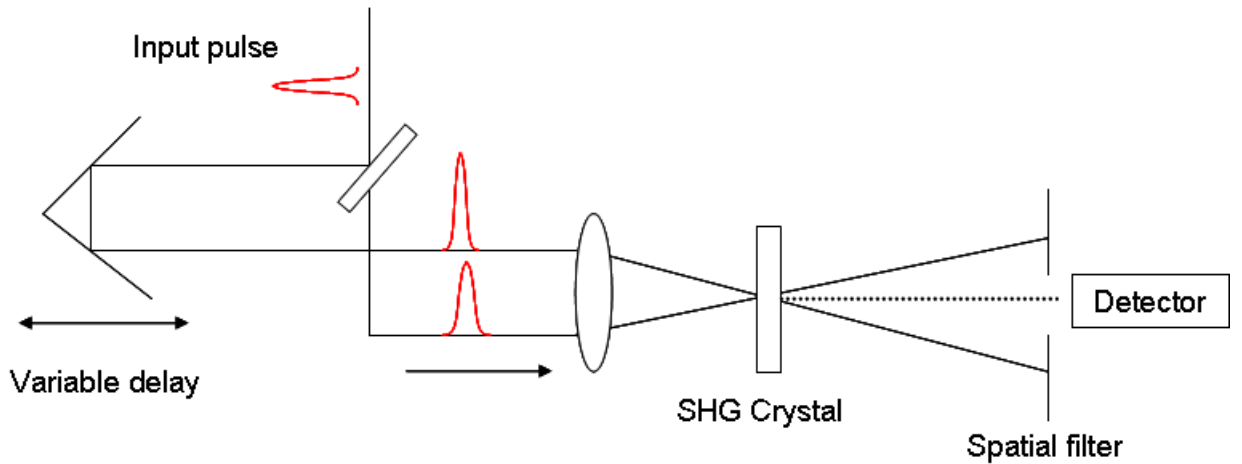


Figure 5.1: Schematic of an intensity autocorrelator

$I(t)$	Δt	$I(\omega)$	$\Delta\omega$	$\Delta\omega\Delta t$	$G_2(\tau)$	$\Delta\tau$	$\Delta\tau/\Delta t$
e^{-t^2}	1.665	$e^{-\omega^2}$	1.665	2.772	$e^{\frac{\tau^2}{2}}$	2.355	1.414
$\text{sech}^2(t)$	1.763	$\text{sech}^2\{\frac{\pi}{2}\omega\}$	1.122	1.978	$\frac{3[\tau \cosh(\tau) - \sinh(\tau)]}{\sinh^3(\tau)}$	2.720	1.543

Table 5.1: Mathematical results for different pulse shapes and their correlation function [3]

5.2 Interferometric Autocorrelation

Interferometric autocorrelation is a variant of the intensity autocorrelator. While the intensity autocorrelator filters out any signal contributed by a single pulse replica, the interferometric autocorrelator uses a collinear geometry as shown the figure 5.3

The input laser beam is split into two and allowed to travel different paths by mounting one of the mirrors (on which the beams will strike) to a loud speaker. This moves the mirror back and forth through a distance x corresponding to a delay time τ . The two pulses are sent collinearly into a photodiode which acts as a second order process. A second harmonic crystal can also be used. A photodiode has the advantage that it is cheaper, and does not have the problem of phase matching [24]. The electrical signal generated is then directed to the oscilloscope. We can calculate the interferometric autocorrelation function. An expression for the interferometric autocorrelation

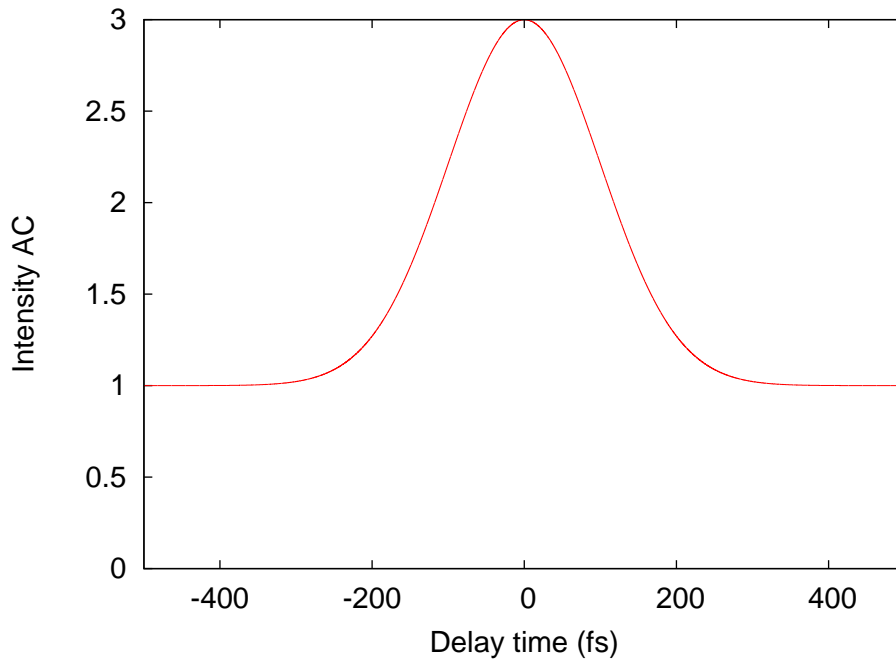


Figure 5.2: Simulated intensity autocorrelation function for Gaussian shaped pulse

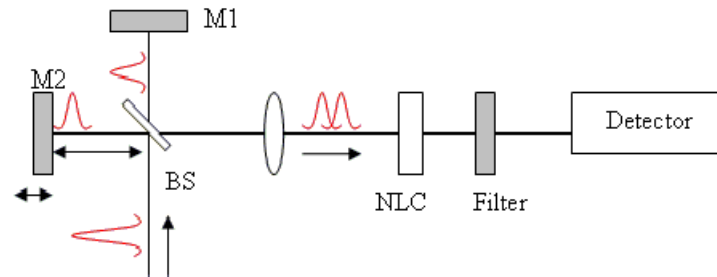


Figure 5.3: Schematic of an interferometric autocorrelator

function will include the pulse width and chirp parameter with the assumption of a pulse shape. The total field after the Michelson interferometer is

the sum of the two identical pulses delayed by τ with respect to each other

$$\begin{aligned} E(t, \tau) &= E(t + \tau) + E(t) \\ &= A(t + \tau)e^{i\omega(t+\tau)} + A(t)e^{i\omega(t)} \end{aligned} \quad (5.4)$$

where $A(t)$ is the complex amplitude, and $e^{i\omega t}$ describes the oscillation with the carrier frequency ω . What we desire to measure is the electric field in time, but since this process is very fast to capture we rather measure the intensity as a function of the delay. The detector integrates over the envelope of the light pulses. After undergoing a second order process, the total signal produced by the interferometric autocorrelator can be written as [25]

$$\begin{aligned} I(\tau) &\propto \int_{-\infty}^{\infty} |(A(t + \tau)e^{i\omega(t+\tau)} + A(t)e^{i\omega(t)})|^2 dt \\ &\propto \int_{-\infty}^{\infty} |A^2(t + \tau)e^{i2\omega(t+\tau)} \\ &\quad + 2A(t + \tau)A(t)e^{i\omega(t+\tau)}e^{i\omega(t)} \\ &\quad + A^2(t)e^{2i\omega(t)}|^2 dt. \end{aligned} \quad (5.5)$$

Taking the absolute square we get

$$\begin{aligned} I(\tau) &\propto \int_{-\infty}^{\infty} [|A(t + \tau)|^4 + 4|A(t + \tau)|^2|A(t)|^2 + |A(t)|^4 \\ &\quad + 2A(t + \tau)|A(t)|^2A^*(t)e^{i\omega\tau} + c.c. \\ &\quad + 2A(t)|A(t + \tau)|^2A^*(t + \tau)e^{-i\omega\tau} + c.c. \\ &\quad + A^2(t + \tau)(A^*(t))^2e^{2i\omega\tau} + c.c.] dt \end{aligned} \quad (5.6)$$

From (5.6), the interferometric autocorrelation function consist of the follow-

ing terms

$$I(\tau) = I_{bs} + I_{intc}(\tau) + I_{\omega}(\tau) + I_{2\omega}(\tau) \quad (5.7)$$

I_{bs} is the background signal, and is a constant with reference to the delay τ as long as the the response time of the detector is much larger than the change in the delay time between the pulses. The expression for the background signal is

$$I_{bs} = \int_{-\infty}^{\infty} (|A(t)|^4 + |A(t + \tau)|^4) dt = 2 \int_{-\infty}^{\infty} I^2 dt \quad (5.8)$$

$I_{intc}(\tau)$ represents the intensity autocorrelation discussed earlier on for non-collinear second harmonic generation and can be expressed as

$$I_{int}(\tau) = 4 \int_{-\infty}^{\infty} |A(t + \tau)|^2 |A(t)|^2 dt = 4 \int_{-\infty}^{\infty} I(t + \tau) I(t) dt \quad (5.9)$$

The coherence term oscillating with ω is denoted by $I(\omega)$ and expressed as

$$I_{\omega}(\tau) = 4 \int_{-\infty}^{\infty} \text{Re} [(I(t) + I(t + \tau)) A^*(t) A(t + \tau) e^{i\omega\tau}] dt \quad (5.10)$$

and the coherence term oscillating with 2ω , $I_{\omega}(2\tau)$ is given by the expression

$$I_{2\omega}(\tau) = 2 \int_{-\infty}^{\infty} \text{Re} [A^2(t) (A^*(t + \tau))^2 e^{2i\omega\tau}] dt \quad (5.11)$$

The interferometric autocorrelation function is normalized relative to the background intensity I_{bs} which gives equation (5.7) as

$$\frac{I(\tau)}{I_{bs}} = I_{Iac}(\tau) = 1 + \frac{I_{int}(\tau)}{I_{bs}} + \frac{I_{\omega}(\tau)}{I_{bs}} + \frac{I_{2\omega}(\tau)}{I_{bs}}. \quad (5.12)$$

The intensity of the second harmonic signal is maximum at $\tau = 0$. For alignment purposes we evaluate the integrals at $\tau = 0$ and $\tau \rightarrow \pm\infty$ with the aim of finding a peak to background ratio of the interferometric autocorrelation

trace

$$\begin{aligned}
 I_{bs} &= 2 \int_{-\infty}^{\infty} |A(t)|^4 \\
 I_{int}(\tau = 0) &= 4 \int_{-\infty}^{\infty} |A(t)|^4 \\
 I_{\omega}(\tau = 0) &= 8 \int_{-\infty}^{\infty} |A(t)|^4 \\
 I_{2\omega}(\tau = 0) &= 2 \int_{-\infty}^{\infty} |A(t)|^4.
 \end{aligned} \tag{5.13}$$

We deduce that

$$\begin{aligned}
 I_{Iac}(\tau) |_{\text{maximum}} = I_{Iac}(0) &= 8 \\
 I_{Iac}(\tau \rightarrow \pm\infty) &= 1
 \end{aligned} \tag{5.14}$$

This 1:8 ratio between the peak and the wings of the interferometric autocorrelation is important and serves as a guide for the alignment of the interferometric autocorrelator. We recall that traditional pulse characterization requires retrieving the pulse duration. It is therefore important to assume an input pulse shape. Once a pulse shape is assumed and inserted into the interferometric autocorrelation, information on the pulse width and chirp parameter can be extracted. If we assume a complex envelope of a Gaussian pulse in the form of equation (5.15)

$$A(t) = \exp \left[-\frac{1}{2} \left(\frac{t}{t_p} \right)^2 (1 + i\beta) \right], \tag{5.15}$$

where t_p is the pulse width and β is some measure of the pulse chirp. Then the theoretical interferometric autocorrelation function assuming the Gaussian pulse envelope can be calculated using (5.15) in equation (5.7). We first find the value for the background signal I_{bs}

$$\int_{-\infty}^{\infty} |A(t + \tau)|^4 dt = t_p \sqrt{\frac{\pi}{2}} \tag{5.16}$$

and

$$\int_{-\infty}^{\infty} |A(t)|^4 dt = t_p \sqrt{\frac{\pi}{2}} \quad (5.17)$$

Therefore from equation (5.8)

$$I_{bs} = \int_{-\infty}^{\infty} (|A(t)|^4 dt + |A(t + \tau)|^4 dt) = t_p \sqrt{\frac{\pi}{2}} \quad (5.18)$$

Now we evaluate the intensity autocorrelation I_{int} of the Gaussian function

$$I_{intc}(\tau) = 4 \int_{-\infty}^{\infty} |A(t + \tau)|^2 |A(t)|^2 dt = 4t_p \sqrt{\frac{\pi}{2}} e^{-\frac{\tau^2}{2t_p^2}} \quad (5.19)$$

so that the second term in equation (5.7) now becomes

$$\frac{I_{int}}{I_{bs}} = \frac{4t_p \sqrt{\frac{\pi}{2}} e^{-\frac{\tau^2}{2t_p^2}}}{2t_p \sqrt{\frac{\pi}{2}}} = 2t_p \sqrt{\frac{\pi}{2}} e^{-\frac{\tau^2}{2t_p^2}} \quad (5.20)$$

The coherence term oscillating with ω ,

$$\begin{aligned} I_{\omega}(\tau) &= 4 \int_{-\infty}^{\infty} \text{Re} [(I(t) + I(t + \tau)) A^*(t) A(t + \tau) e^{i\omega\tau}] dt \\ &= 8t_p \sqrt{\frac{\pi}{2}} e^{-\frac{3 + \beta^2}{8} \left(\frac{\tau}{t_p}\right)^2} \cos(\omega\tau) \cos\left(\frac{\beta}{4} \left(\frac{\tau}{t_p}\right)^2\right) \end{aligned} \quad (5.21)$$

and the third term in (5.7) becomes

$$\begin{aligned} \frac{I_{\omega}(\tau)}{I_{bs}} &= \frac{8t_p \sqrt{\frac{\pi}{2}} e^{-\frac{3 + \beta^2}{8} \left(\frac{\tau}{t_p}\right)^2} \cos(\omega\tau) \cos\left(\frac{\beta}{4} \left(\frac{\tau}{t_p}\right)^2\right)}{2t_p \sqrt{\frac{\pi}{2}}} \\ &= 4e^{-\frac{3 + \beta^2}{8} \left(\frac{\tau}{t_p}\right)^2} \cos(\omega\tau) \cos\left(\frac{\beta}{4} \left(\frac{\tau}{t_p}\right)^2\right) \end{aligned} \quad (5.22)$$

Finally we evaluate the coherence term at 2ω

$$\begin{aligned} I_{2\omega}(\tau) &= 2 \int_{-\infty}^{\infty} \operatorname{Re} [A^2(t) (A^*(t + \tau))^2 e^{2i\omega\tau}] dt \\ &= \sqrt{2\pi} t_p e^{-\frac{\beta^2 \tau^2}{2t_p^2} - \frac{\tau^2}{2t_p^2}} \cos(2\tau\omega) \end{aligned} \quad (5.23)$$

and the fourth term in equation (5.7) becomes

$$\begin{aligned} \frac{I_{2\omega}(\tau)}{I_{bs}} &= \frac{\sqrt{2\pi} t_p e^{-\frac{\beta^2 \tau^2}{2t_p^2} - \frac{\tau^2}{2t_p^2}} \cos(2\tau\omega)}{2t_p \sqrt{\frac{\pi}{2}}} \\ &= e^{-\frac{\beta^2 \tau^2}{2t_p^2} - \frac{\tau^2}{2t_p^2}} \cos(2\tau\omega) \end{aligned} \quad (5.24)$$

The theoretical calculation of the interference autocorrelation function for a Gaussian pulse then turns out to be

$$\begin{aligned} I_{Iac}(\tau) &= 1 + \left(2 + e^{-\frac{\beta^2}{2} \left(\frac{\tau}{t_p}\right)^2} \cos(2\omega\tau) \right) e^{-\frac{1}{2} \left(\frac{\tau}{t_p}\right)^2} \\ &+ 4e^{-\frac{3 + \beta^2}{8} \left(\frac{\tau}{t_p}\right)^2} \cos\left(\frac{\beta}{4} \left(\frac{\tau}{t_p}\right)^2\right) \cos(\omega\tau) \end{aligned} \quad (5.25)$$

The autocorrelation function is plotted in figures 5.4 and 5.5 with different values of β . Analysis of equation (5.25) gives the pulse width t_p and the chirp parameter β [25].

The intensity and interferometric autocorrelation techniques are limited by their symmetric nature when second harmonic generation is been utilized. To overcome this, third harmonic generation can be used. Another limitation of intensity and interferometric autocorrelation is the inability to recover the phase of the input pulse. However, if the pulse duration is desired but the

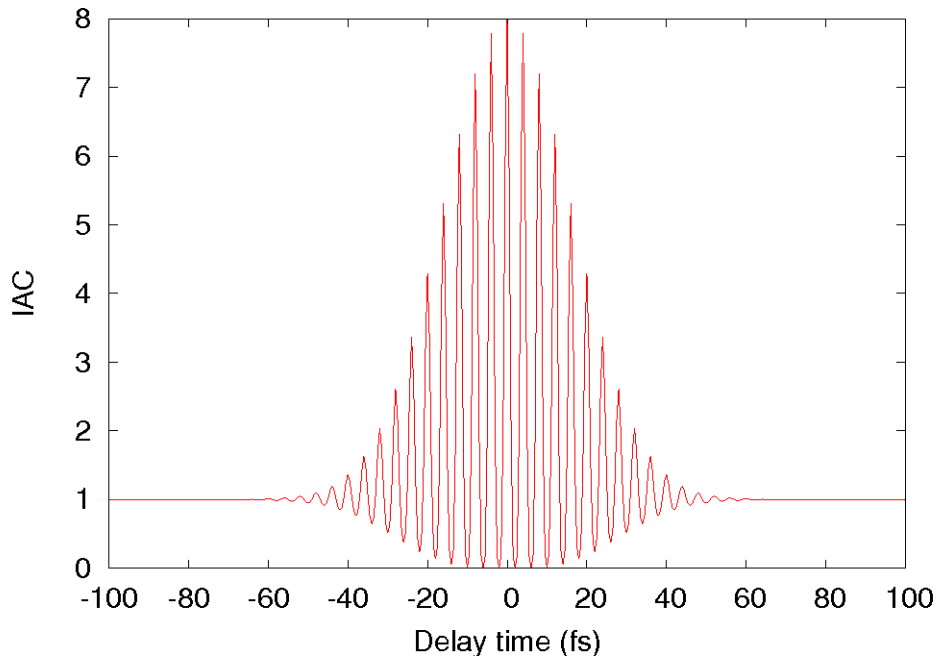


Figure 5.4: Theoretical interferometric autocorrelation trace for a Gaussian shaped pulse with no chirp $\beta = 0$

symmetry of the pulse shape and input pulse phase are insignificant for a particular measurement then these traditional correlation techniques will be the best option to use for measurement. It has the advantage that it is simpler to implement since its implementation basically requires a nonlinear crystal, some mirrors and a photomultiplier tube [26].

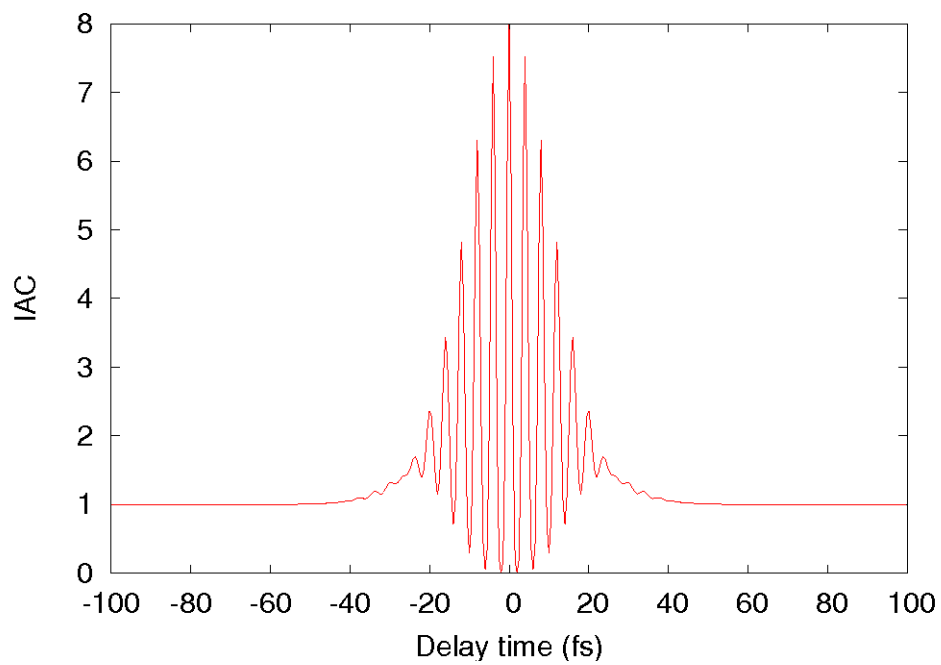


Figure 5.5: Theoretical interferometric autocorrelation trace for a Gaussian shaped pulse with chirp parameter, $b = 2$

6. Spectral Interferometry

Spectral interferometry relies on frequency domain interferences between two light pulses which are delayed in time with respect to each other [27]. Analysis of the spectral interferogram of these two beams provides in a purely algebraic way the spectral phase difference between the two light pulses. Spectral interferometry converts phase information that would otherwise be impractical to retrieve into amplitude information that can be read using a square law detector [28]. For the next few sections we shall see how the spectral interference of two electric field distributions recorded by a square law detector can be used to retrieve the phase of an incident electric field.

6.1 Fourier Transform Spectral Interferometry

Fourier transform spectral interferometry (FTSI) involves the spectral interference of two electric fields delayed in time known as the test and reference pulses. The principle of FTSI has found many applications including the complete characterization of optical short pulses. It is not a self referencing technique, meaning that it requires a well characterized reference pulse. When compared with most time domain interference techniques, FTSI has the advantage of simplicity [29]. It is a single shot technique meaning that there are no moving parts in the experimental set up. A single shot data is adequate to provide all the information required about a pulse. One main advantage of FTSI when compared with other interferometric techniques is that it can be used in the characterization of ultra weak, ultrashort, laser pulses since it does not need a nonlinear interaction for its operation [30]. In reference [30], the authors characterized the reference pulse using frequency resolved optical gating and FTSI was used to characterize the unknown pulse. By measuring the spectrum of the sum of the known (strong) pulse and the unknown (ultraweak) pulse, the unknown weak pulse is fully characterized. This technique is termed TADPOLE (Temporal analysis by dispersing a pair of light electric field) [31].

6.2 Principle of FTSI

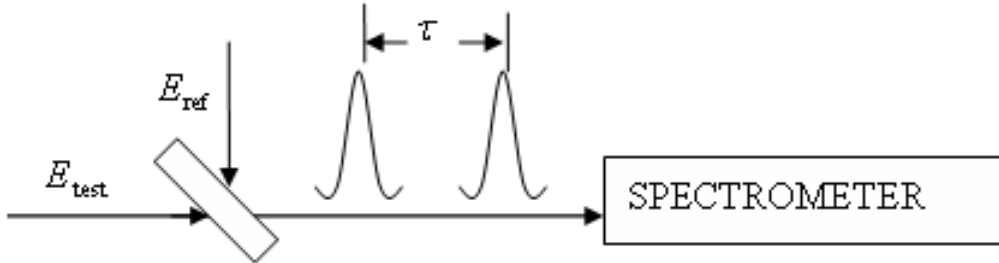


Figure 6.1: Schematic of a typical Fourier transform spectral interferometry set up

Given the frequency dependent test and reference electric field as $\sqrt{I_{\text{test}}}(\omega) \exp(i\phi_{\text{test}}(\omega))$ and $\sqrt{I_{\text{ref}}}(\omega) \exp(i\phi_{\text{ref}}(\omega))$ respectively, where ϕ_{test} and ϕ_{ref} is the phase of the test and reference pulse respectively. Introducing a delay τ between the two fields, the total electric field spectrally resolved with a spectrometer is given by [27]

$$S(\omega) = I_{\text{test}}(\omega) + I_{\text{ref}}(\omega) + 2\sqrt{I_{\text{test}}}(\omega)\sqrt{I_{\text{ref}}}(\omega) \cos(\phi_{\text{test}}(\omega) - \phi_{\text{ref}}(\omega) + \omega\tau) \quad (6.1)$$

The interferogram contains three main terms. The first two terms are just the power spectra of the incident beams and do not contain the interference part of the signal. The last term contains the interference part and indeed the phase difference of the two input pulses. A Fourier transform of the measured signal to a pseudo time domain, isolating one of the side bands containing the spectral phase difference and concatenation reveals the desired phase of the test pulse. The full analysis of this procedure will be illustrated in the SPIDER technique (Chapter 7). FTSI can also be used to retrieve the phase transfer function of optical materials or linear dispersion introduced. If the delay between the two pulses are created using a Michelson type set up, the phase difference will be as a result of the difference in the magnitude of the dispersion experienced by the pulses in the arms of the interferometer. In cases where an etalon is used to create a delay between two replicas, FTSI

can also be used to measure the linear dispersion of the material.

6.3 Experimental results of FTSI

For this work we conducted a simple FTSI experiment to measure the phase transfer function of BK7 glass plate [32]. The phase difference between the pulses is due to the propagation of one replica of the input pulse through the glass plate. We used a pulse replica generated from the first two reflections off an uncoated BK7 glass plate of about $140\ \mu\text{m}$ thickness. Though as expected there are multiple reflections from the glass plate but since their energies are much lower than the first two, the effect is insignificant. The measured interference spectra of both the fundamental and the second harmonic spectra were recorded (Figure 6.2). The available spectrometer that records the

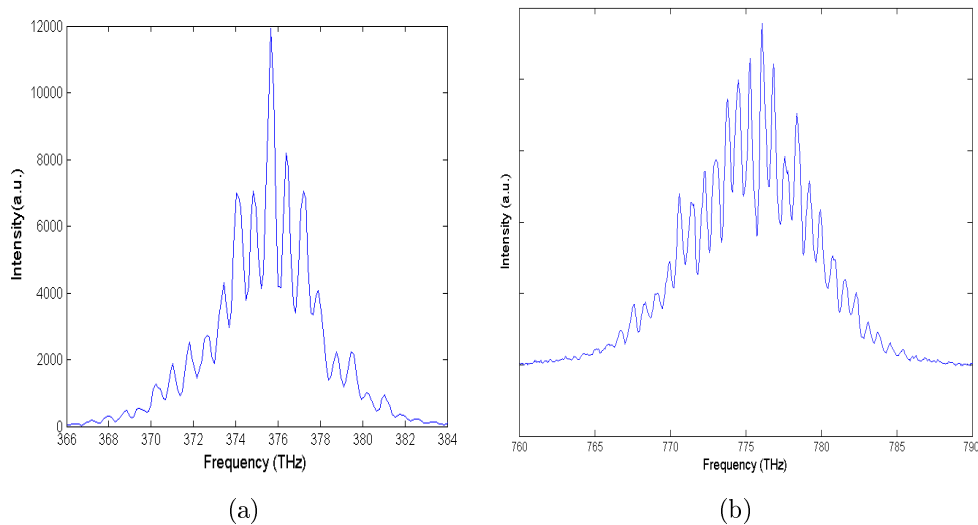


Figure 6.2: (a) Measured spectral interference for two replicas created from the reflection off an uncoated glass plate (b) Measured interference spectra of two frequency doubled replicas

wavelength range of the second harmonic beam has a higher resolution so for analysis we used the second harmonic spectral interferogram. An inversion routine was applied to the interferogram to retrieve the spectral phase shift

function as a result of the dispersion through the length of the glass plate. The process involves Fourier transforms and analysis just as in SPIDER. Using a similar inversion routine which will be explained in detail in the next

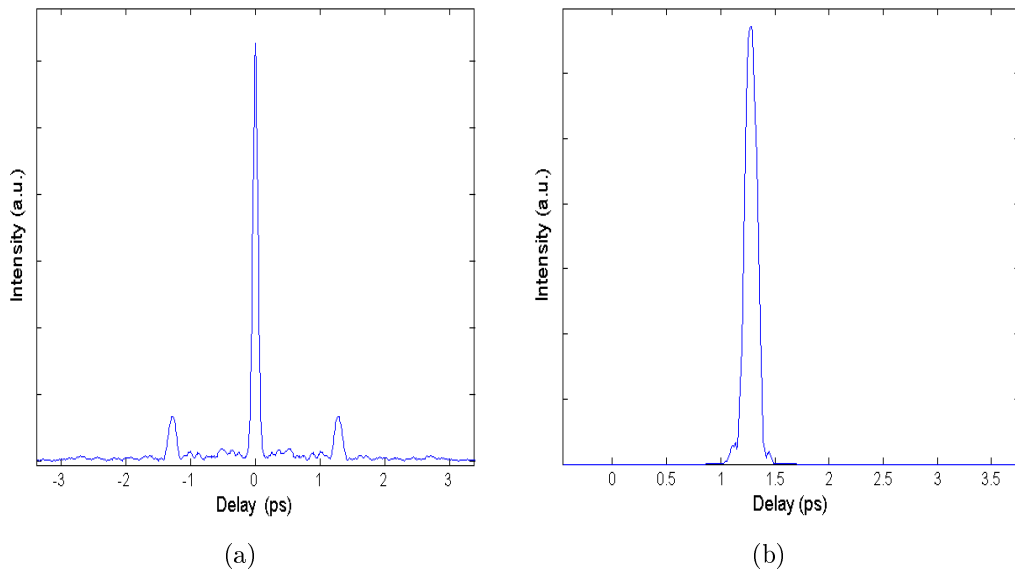


Figure 6.3: (a) Inverse Fourier transform of (6.2) (b) Filtered positive side lobe

chapter, the phase difference, usually called the phase transfer function is retrieved from the interferogram.

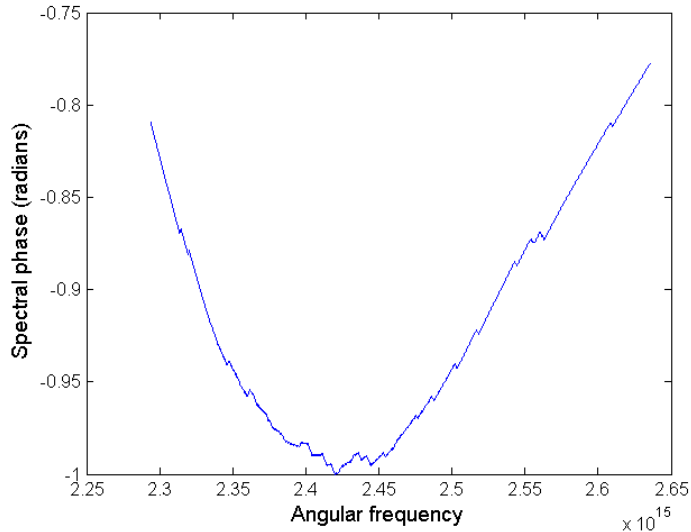


Figure 6.4: Phase transfer function retrieved for about $1.4 \mu\text{m}$ glass plate using FTSI

6.4 Spectral shearing interferometry

A more convenient way of obtaining a reference pulse is to generate a shear between replicas of the test pulse. Creating a shear involves shifting the center frequencies of two pulse replicas each by a unique amount. This can be done by sending the replicas through a phase modulator [33]. The authors in [33] demonstrated how an electro-optic temporal phase modulator can be used to generate an adequate spectral shear for sub-picosecond pulses. Note that for spectral shearing interferometry, unlike FSTI, is a self referencing technique and is highly sensitive since it involves no nonlinear optics. Though test plus reference pulse characterization techniques can offer better sensitivity, self referencing temporal diagnostics with a better sensitivity will be valuable in applications such as optical telecommunication or phase-sensitive detection of nonlinear polarization induced emission, where nonlinear optics can not be achieved as a result of the low power level pulses used [34]. However, linear spectral shearing interferometry using linear phase modulators is not ideal for characterizing much shorter pulses as a few picoseconds. Such ultrashort pulses have very broad bandwidths making it difficult to find a

phase modulator capable of generating an appropriate spectral shear. For the most common pulse lengths of about 10 fs up to 1 ps generating the frequency shear involves nonlinear optics, and the easiest way to shift the center frequency without distorting the phase is to sum its broad spectrum with a quasi monochromatic beam and this can be achieved by mixing the unknown pulse with a quasimonochromatic beam in a sum-frequency generation crystal [35]. The SPIDER technique demonstrated in chapter 7 works with this principle.

7. Spectral Phase Interferometry for Direct Electric Field Reconstruction (SPIDER)

Spectral phase interferometry for direct electric field reconstruction is a single shot technique that has successfully been used to retrieve the intensity and phase of ultrashort pulses of up to a few femtoseconds, thereby fully characterizing the pulse. It is a self referencing technique, and a shear is generated between two replicas of the test pulse by superimposing the replicas with a highly chirped pulse in a nonlinear crystal (figure 7.1). A spectral interference pattern is recorded in a spectrometer, analyzed and phase information is retrieved from the interferogram.

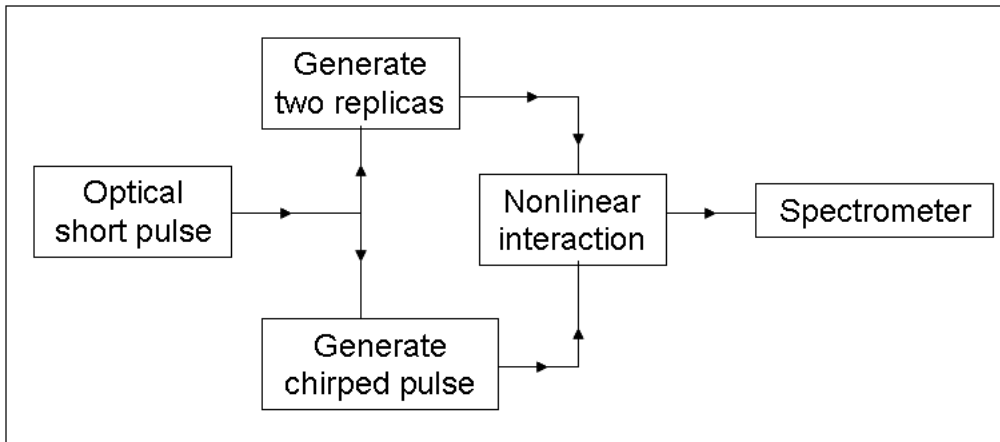


Figure 7.1: Basic components of a SPIDER set up

The short pulse to be measured is directed to strike a glass plate or etalon and two replicas are generated from the first two Fresnel reflections of the glass. In general beam splitters can be used to generate the replica with the advantage that the delay can be varied at will [12]. For this project an etalon has been used and the round trip time of the etalon determined the delay. The etalon or glass plate offers a high mechanical stability and

easier alignment. The transmitted beam is directed to a setup of an optical stretcher, which could be a pair of gratings or a dispersive glass block. Here also one advantage of the grating stretcher over the glass stretcher is that the dispersion induced by the grating can be varied by adjusting the separation between the two gratings. For our set up a grating stretcher is used.

7.1 Optimization parameters

The key to the SPIDER technique is the generation of the spectrally sheared pulse pair, and the resolution of the temporarily separated pulse pair with a spectrometer [36]. For this to happen with the SPIDER technique, the delay between the replicas, the amount of dispersion induced by the stretcher and the nonlinear interaction has to be carefully considered.

7.1.1 Generating the replica

The delay time τ between the pulses should be chosen carefully. In our case the round trip time of light in the glass etalon is given by

$$\tau = \frac{2\eta l}{c} \quad (7.1)$$

determined the delay. Here l is the thickness of the glass and η is the refractive index. The magnitude of the spectral shear Ω is not independent of the delay [37]

$$\Omega = -\frac{\tau}{2\phi''} \quad (7.2)$$

where ϕ'' is the group delay dispersion of the chirped pulse. The pulses should be sufficiently separated in time as to avoid any temporal overlap between them, at the same time it should satisfy the Nyquist criterion, with the condition that the available spectrometer should be able to resolve more than two points per fringe. We note also that the process to retrieve the pulse intensity and phase depends on whether the pulses are been sufficiently separated in time to distinguish between the terms in the interferogram. An ideal

thing to do, will be to choose a time delay that is about 10 times the transform limited pulse duration, this will ensure no temporal overlap between the pulses and proper filtering of the side band after the spectral interferogram has been Fourier transformed. For this work we used the reflections off a $140\ \mu\text{m}$ thickness glass plate that generated a delay of about 1.4 ps.

7.1.2 Generating the chirped pulse

A grating pair is used in generating the chirped pulse. The arrangement is similar to that shown in figure (7.2). The incoming light strikes the first

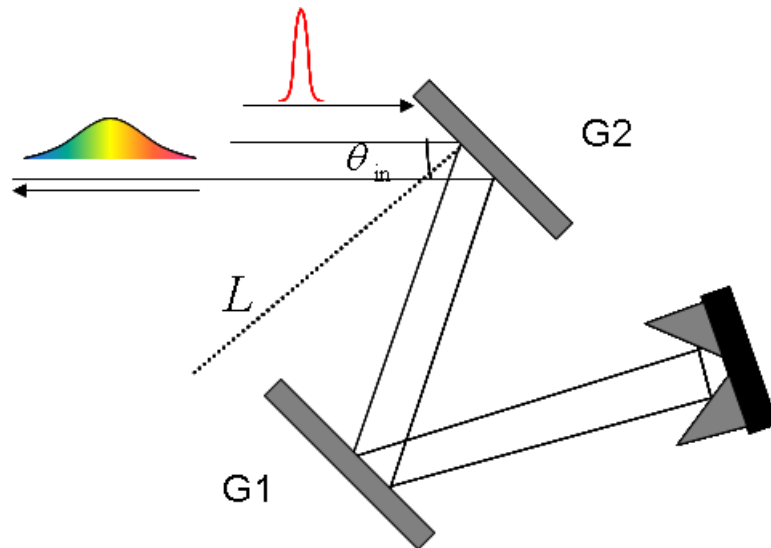


Figure 7.2: Schematic of a grating optical disperser used for stretching ultrashort pulses

grating at an angle of incidence θ_{in} . The grating disperses the light into its different spectral components. The geometry of the grating is arranged in such a way that longer wavelengths travel longer distances compared to the shorter ones and this induces path length dispersion which stretches the pulse. The spectral shear created also depends on the amount of group delay dispersion (GDD) induced on the chirped pulse ignoring higher orders of dispersion such as Third Order Dispersion (TOD) and Fourth Order Dispersion (FOD). In generating the chirped pulse we bear in mind that we want to

stretch the input pulse relatively long, so that for the duration of the input pulse there is no significant variation frequency in the stretched pulse. This ensures that each of the pulse replicas mixes with a unique quasi monochromatic component of the chirped pulse [38]. For our set up, since we used a glass plate to generate the delay, our delay was fixed and the spectral shear created could only be monitored by adjusting the second order dispersion on the chirped pulse. This is done by adjusting the separation L between the two gratings. When the stretched pulse is generated using a pair of gratings, the value of the second order dispersion or group delay dispersion induced by the grating can be calculated analytically as [39]

$$\phi'' = \frac{\lambda^3 L}{2\pi c^2 d^2} \left[1 - \left(\frac{\lambda}{d} - \sin \theta_{\text{in}} \right)^2 \right]^{-3/2} \quad (7.3)$$

or in frequency,

$$\phi'' = \frac{4\pi^2 c L}{\omega^3 d^2} \left[1 - \left(\frac{2\pi c}{\omega d} - \sin \theta_{\text{in}} \right)^2 \right]^{-3/2} \quad (7.4)$$

For our set up, we kept the incidence angle θ_{in} at 37° , the separation between the gratings was 9.3 cm, the grating used are ruled at $d = 1200/\text{mm}$ lines, the spectral width of the input pulse was about $2\pi \times 6.489$ THz, and we were working at a central wavelength of 775 nm. With these parameters we calculated the second order dispersion from the stretcher to be 2.5877 fs^2 . The stretched pulse duration was also estimated using the formula $T_{\text{stretched}} = \Delta\omega\phi''$, which resulted in a duration of about 11 ps and the shear generated was about 5.4 THz. Figure 7.3 is a plot of the gradual increase of the stretched pulse duration with distance between the grating pair [40].

The relationship between the stretched pulse duration and grating pair separation is linear. This illustrates pulse broadening as a result of the difference in the optical path of the different spectral components of the pulse.

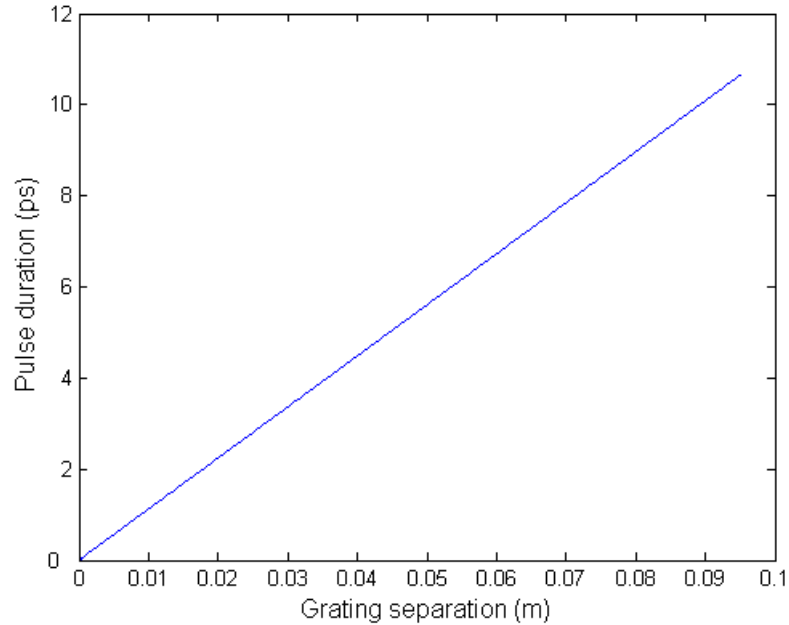


Figure 7.3: Increase in the stretched pulse duration with grating pair separation

7.1.3 Nonlinear Interaction

The pulse replicas from the interferometer are superimposed on the stretched pulse from the grating stretcher in a birefringent nonlinear crystal. The crystal Beta barium borate BBO is used in this case, with thickness of about $100 \mu\text{m}$. A noncollinear geometry illustrated in figure 4.4 is used. When these three pulses mix in the crystal, there are three possible outputs. Two of them are due to second harmonic generation in which case two photons from the same beam combine to produce a beam with twice its frequency ($\omega_1 + \omega_1 = 2\omega_1$, $\omega_2 + \omega_2 = 2\omega_2$). The other output, which is the important one in this case, is the sum frequency generated pulse, where one photon from each of the input pulse sums up to to produce a beam representing the two frequencies ($\omega_1 + \omega_2 = \omega_3$). An aperture is used to select the sum frequency beam. The interferogram is recorded by a spectrometer. The second harmonic generation without the shear, is also recorded as a calibration trace using the same noncollinear geometry [9].

7.2 SPIDER Theory

Assume we have already generated replicas of a pulse that have each experienced a unique frequency shift. The shear created as a result of the frequency shifting process is then (see figure 7.4),

$$\Omega = \Omega_2 - \Omega_1 \quad (7.5)$$

where Ω_1 is the new centre frequency of the first frequency shifted replica and Ω_2 is the centre frequency of the second frequency shifted replica.

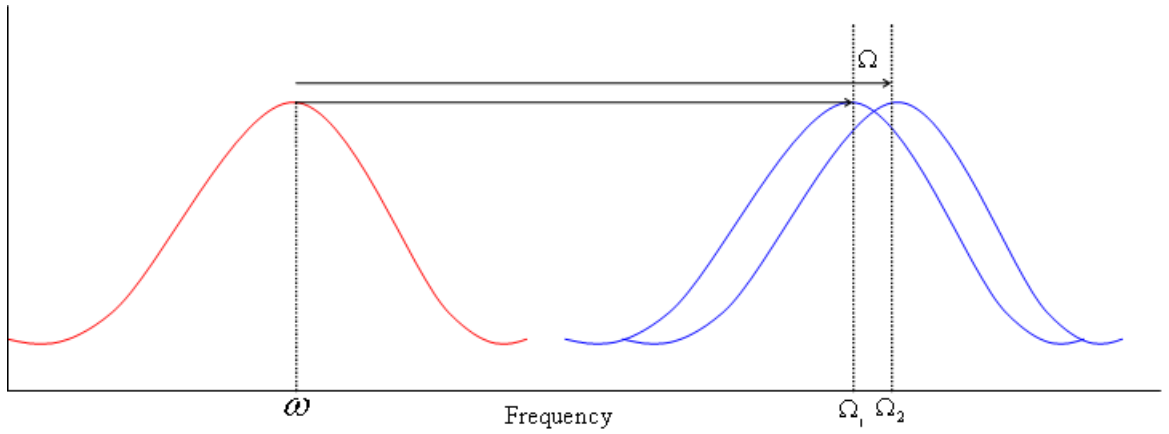


Figure 7.4: Schematic of the frequency shifting process used for the SPIDER technique

Mathematically, we can express the frequency shifted pulse replicas entering the spectrometer in the frequency domain, with respect to each other, as

$$\sqrt{I(\omega)} \exp(i\phi(\omega))$$

and

$$\sqrt{I(\omega + \Omega)} \exp(i(\phi(\omega + \Omega) + \omega\tau))$$

where τ is the temporal delay between the pulses. The interferogram of the

two signals is then

$$S(\omega, \tau) = |\sqrt{I(\omega)} \exp(i\phi(\omega)) + \sqrt{I(\omega + \Omega)} \exp(i\phi(\omega + \Omega) + \omega\tau)|^2 \quad (7.6)$$

which gives after using some trigonometrical identities

$$S(\omega) = I(\omega) + I(\omega + \Omega) + 2\sqrt{I(\omega)}\sqrt{I(\omega + \Omega)} \cos(\phi(\omega) - \phi(\omega + \Omega) + \omega\tau) \quad (7.7)$$

Already we can see from the expression above that backbone of the SPIDER techniques revolves around creating the spectral shear.

For reference purposes and simplicity we can rewrite equation (7.7) as

$$S(\omega) = D^{dc}(\omega) + \exp(-i\tau\omega)D^{-ac}(\omega) + \exp(i\tau\omega) \times D^{+ac}(\omega) \quad (7.8)$$

where

$$D^{dc}(\omega) = |E(\omega + \Omega)|^2 + |E(\omega)|^2 \quad (7.9)$$

and

$$D^{\pm ac}(\omega) = |E(\omega - \Omega)E(\omega)| \exp[\pm i(\phi(\omega - \Omega) - \phi(\omega))] \quad (7.10)$$

The $D^{dc}(\omega)$ term which represents the first two terms in equation (7.7) is the sum of the individual spectra of the two frequency shifted pulses and contain no phase information. The other two terms each contains the desired phase information. The inverse Fourier transform of $S(\omega)$ is calculated and one of the side bands is easily filtered if the delay between the replicas is large enough. The filtered lobe is Fourier transformed back to frequency domain and the argument retrieved is in the form of equation (7.11)

$$\arg(D^{+ac}(\omega)) = \phi(\omega) - \phi(\omega + \Omega) + \omega\tau \quad (7.11)$$

The linear phase term $\omega\tau$ is subtracted by direct measurement. This is done by recording the spectral interferogram of the pulse pair without the spectral shear. When the noncollinear geometry is used the second harmonic interference signal with contribution from only the pulse replicas is easily

identified and recorded. Once the linear term is subtracted, what remains is the spectral phase difference in the form

$$\Delta\phi_s(\omega) = \phi(\omega) - \phi(\omega + \Omega) \quad (7.12)$$

At this stage, the spectral phase can be recovered either by integration or concatenation. Integration uses the principle of *Newtons difference quotient*, so that if the shear generated is small enough relative to the structure of the spectral phase, then the phase difference is the first derivative of the spectral phase multiplied by the shear, that is

$$\Delta\phi_s(\omega) = \phi(\omega) - \phi(\omega + \Omega) \approx \Omega \frac{d\phi(\omega)}{d\omega} \quad (7.13)$$

so that the spectral phase can be reconstructed by integration

$$\phi(\omega) \approx \frac{1}{\omega} \int \Delta\phi_s(\omega) d\omega \quad (7.14)$$

The integration method has the advantage that it provides a simple means of averaging over the many data sets recorded in a single interferogram. The other method of reconstructing the spectral phase from the spectral phase difference is by concatenation. The phase at frequencies $\omega + \Omega$ is found from the phase at frequency ω by simply subtracting the two SPIDER phases at these frequencies [37]. In practice, the phase at some center frequency say ω_0 is set equal to zero, so that

$$\phi(\omega_0 - \Omega) = -\Delta\phi_s(\omega_0)$$

we can then write the phase at a discrete set of frequencies (that is the phase at frequencies separated by the shear) $\omega_0 \pm n\Omega$ where n is an integer as [41]

$$\begin{aligned}
& \vdots & (7.15) \\
\phi(\omega_0 - 2\Omega) &= \Delta\phi_s(\omega_0 - 2\Omega) + \Delta\phi_s(\omega_0 - \Omega) \\
\phi(\omega_0 - \Omega) &= \Delta\phi_s(\omega_0 - \Omega) \\
\phi(\omega_0) &= 0 \\
\phi(\omega_0 + \Omega) &= -\Delta\phi_s(\omega_0) \\
\phi(\omega_0 + 2\Omega) &= -\Delta\phi_s(\omega_0 + \Omega) \\
& \vdots & (7.16)
\end{aligned}$$

It is seen more clearly here that the choice for Ω is important, and one advantage of using the concatenation technique is that it allows under sampling to be easily recognized. The spectral phase for frequencies separated by the spectral shear is retrieved by adding up the phase differences. The last step in reconstructing the electric field of the input pulse is to determine the spectral amplitude, $|E(\omega)|$. This can be done from a separate measurement of the spectral intensity of the input pulse using a spectrometer, it can also be retrieved from the $D^{dc}(\omega)$ term in equation (7.8). The spectral amplitude combined with the reconstructed spectral phase thus fully recovers the input pulse. For this work we analyzed phase using both the integration and concatenation procedures.

A concise step to step SPIDER inversion routine used for retrieving the input temporal intensity and phase is shown in figure 7.5 [41]. The Matlab code for the SPIDER inversion routine that was developed during this project and applied is given in appendix A.3.

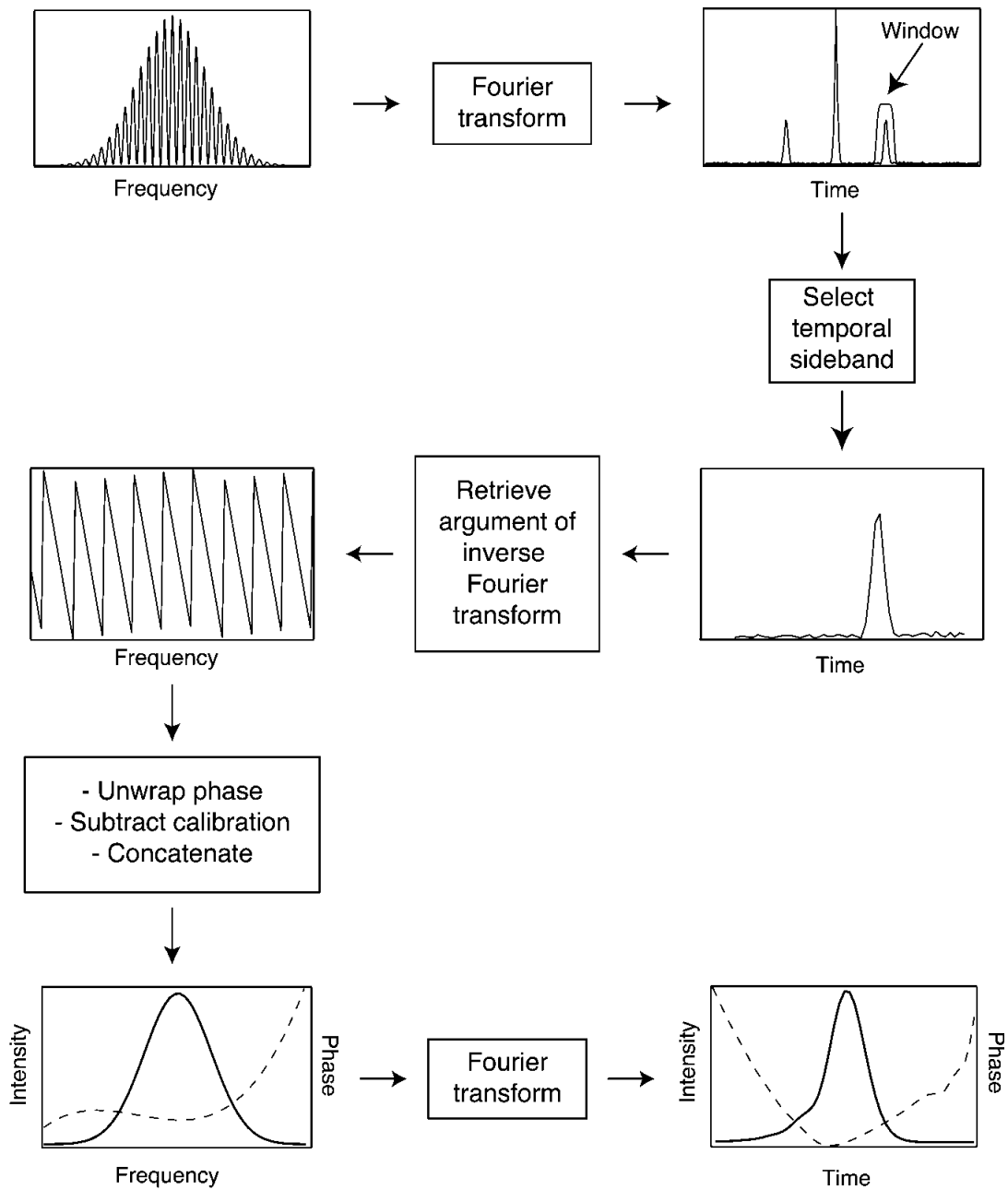


Figure 7.5: SPIDER inversion routine algorithm

7.3 Experimental implementation, results and discussion

The main SPIDER setup was built on a 24×54 cm bread board mounted firmly on an optical table. The setup is illustrated in figure 7.6, and the

picture of the SPIDER setup is shown in figure 7.16. The pulse to be characterized emerged from a Ti:sapphire modelocked oscillator tuned to a central wavelength of 775 nm. An iris is used to ensure a consistent direction of the input beam. The beam strikes the glass plate GP creating two replicas from its first and second reflections. The transmitted beam travels directly to a reflective grating G1, the grating disperses the beam and is reflected from G2 to a double right angled prism arrangement. Here the beam is displaced spatially (vertically), follows the same path back and is picked up by a pick up mirror M1 which steers the stretched pulse to a reflective right angle prism that sends this beam parallel to the pulse pair. The reflections from the glass plate GP is steered along the path M2, M3, M4, M5 and M6 which sends the pulse pair parallel to the stretched pulse. It is necessary that the stretched pulse and pulse pair overlap in time, so the path of the pulse pair is delayed by the optical path length through M2, M3, M4, M5 and M6, the translation stages T1 and T2 are also used to adjust the optical path length difference of the stretched pulse and the pulse pair. The stretched pulse and the pulse pair are focused with a lens of about 100 mm focal length on a type 1 BBO crystal. The SPIDER signal was then recorded with a USB2000, Ocean Optics high resolution spectrometer.

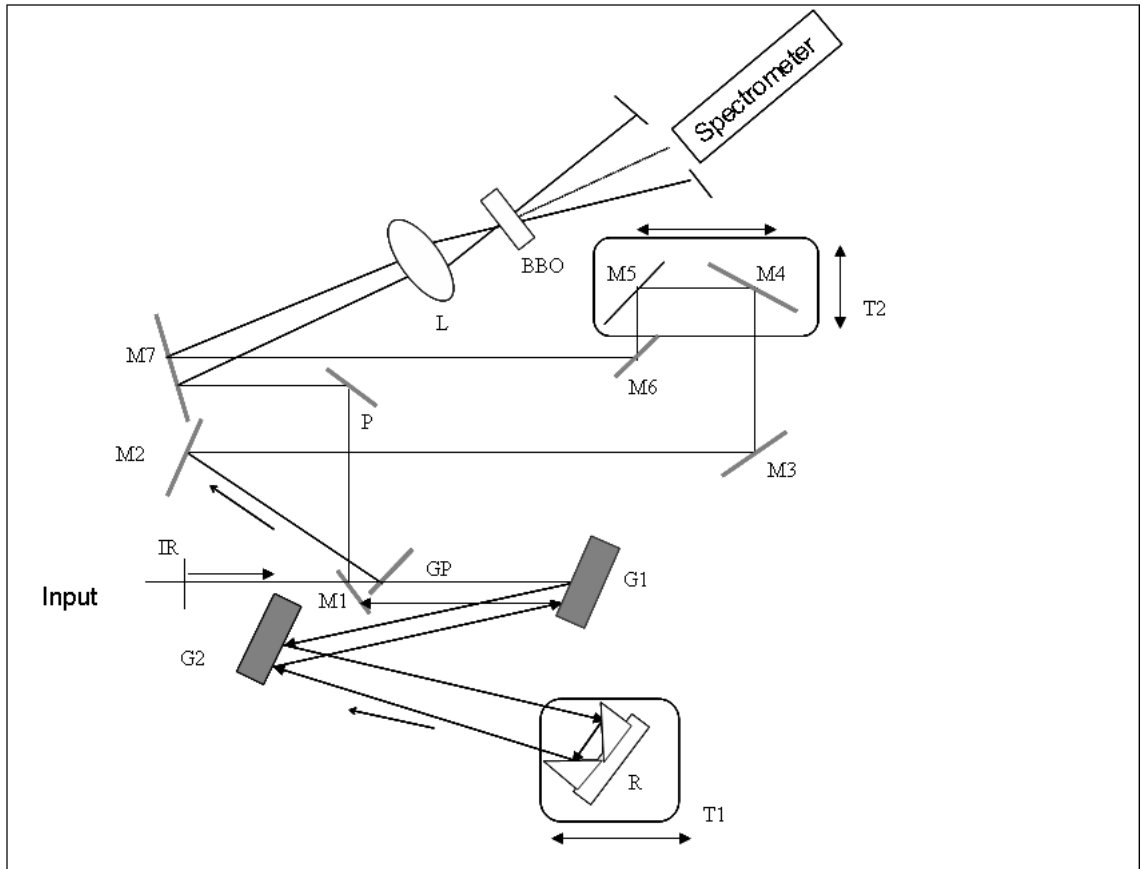


Figure 7.6: Experimental layout of the SPIDER setup: IR-iris, GP-Glass plate, R-reflector, M-Mirrows, P-Gold coated right angled prism, T-translation stages, G-Gratings, L-Lens, BBO-Beta-barium borate nonlinear crystal

The input pulse spectrum was measured and fitted with a Gaussian profile and the fitting parameters provided the central wavelength as $775.59 \text{ nm} \pm 0.016657$ and full width at half maximum $12.2175 \text{ nm} \pm 0.0359$. The spectral width was then calculated. Using the relation

$$\nu = \frac{c}{\lambda} \quad d\nu = \frac{-c}{\lambda^2} d\lambda \quad (7.17)$$

where ν is the center frequency and λ is the center wavelength. The spectral width $d\nu$ which we have earlier denoted as $\Delta\nu$ gives the spectral width as $\Delta\nu = 6.489 \text{ THz}$ and the angular frequency $\Delta\omega = 2\pi \times 6.489 \text{ THz}$.

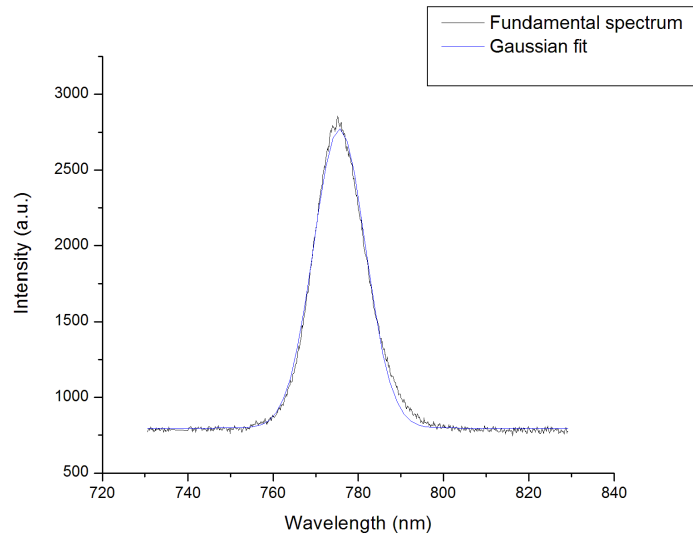


Figure 7.7: Input fundamental spectrum with Gaussian fit

The group delay dispersion of the grating was calculated from equation (7.3) to be $2.5877 \times 10^5 \text{ fs}^2$, and this together with the delay generated a shear of about 5.4103 THz. The measured SPIDER trace, recorded with a USB2000. Ocean Optics high resolution spectrometer, is shown in figure (7.8).

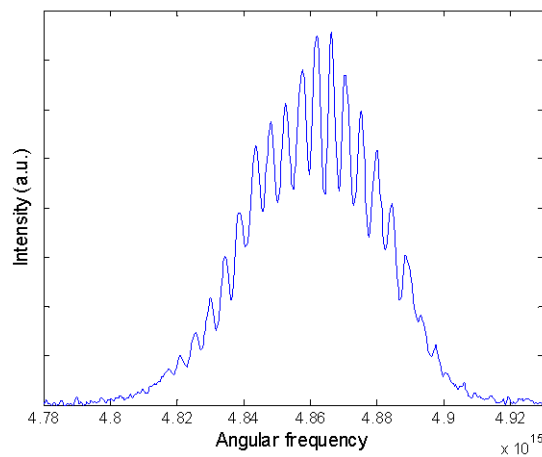


Figure 7.8: Measured SPIDER interferogram (spidergram), phase information of the input pulse is converted to amplitude information

As the SPIDER inversion routine suggests the first step in retrieving the spectral phase is to take the Fourier transform of the SPIDER interferogram. See figure (7.9)

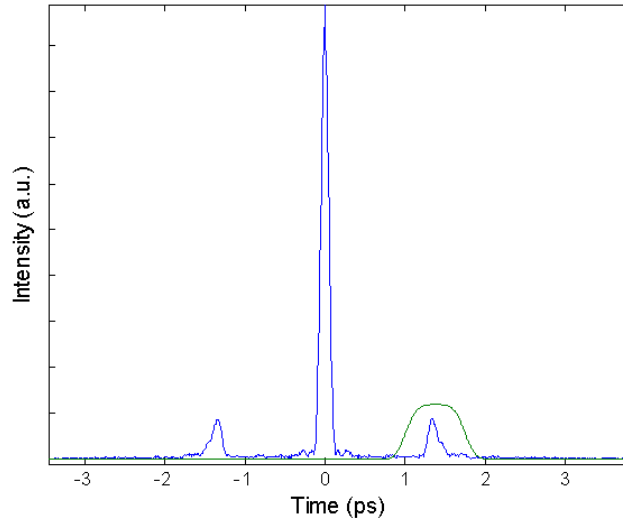


Figure 7.9: Inverse Fourier transform of the measured SPIDER interferogram. Side lobes are centred around the delay of the replicas

We also recorded the interference of the second harmonic signal, in order to subtract the linear term as explained in equation (7.11), and the second harmonic signal without the shear is analyzed to retrieve the linear term with the same SPIDER inversion routine. There are advantages of removing this term in this way as compared removing it numerically. First, it makes the SPIDER set up a low dispersive device since some of the effect of dispersion from the glass plate imparted on the replica that travels through it is removed. Directly measuring the linear phase contribution is also very accurate since the calibration uses the same pair of pulses that has traveled through the SPIDER set up [38].

The inversion routine as laid out in figure 7.5 was carried out on the SPIDER interferogram. The shear generated which is about 12 percent of the spectral width was adequate enough to reconstruct the test pulse phase. There were key parameters that needed to be optimized in the algorithm. The exact

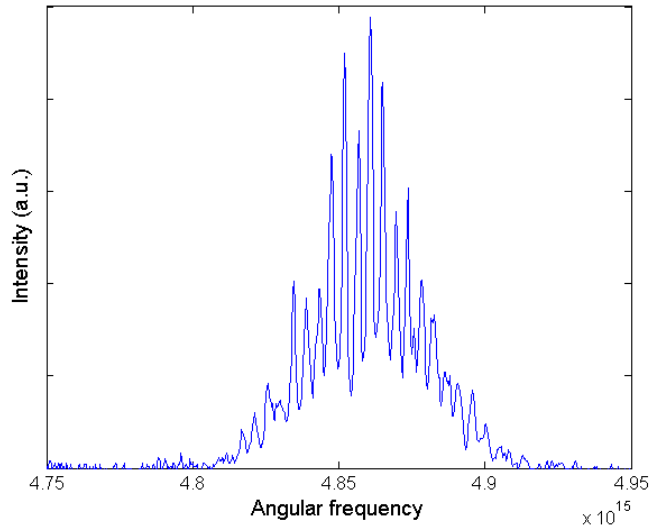


Figure 7.10: Measured calibration trace used for the inversion routine of the SPIDER interferogram

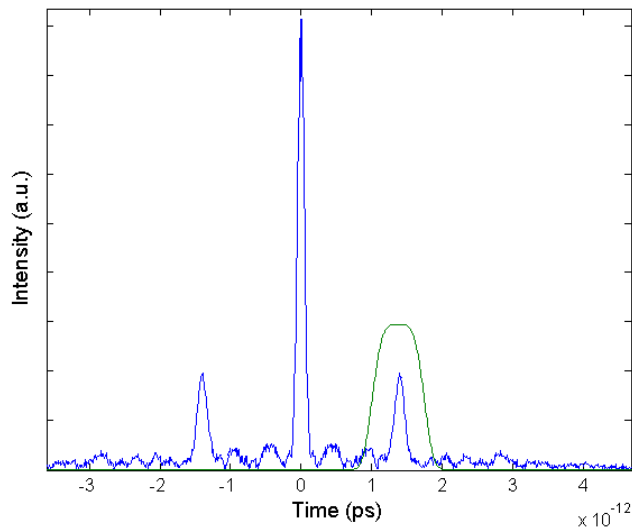


Figure 7.11: Fourier transform of the recorded calibration trace used in the SPIDER algorithm

value of the shear generated needs to be calculated correctly, since we used a grating pair to generate the stretched pulse we simply used equation (7.2) to determine this value. We however ran the algorithm for values of the

shear close to the calculated one to cater for approximations in the calculations. Another parameter that influenced the reconstruction algorithm was the window width used to select a side band from the Fourier transform of the SPIDER Interferogram. For too wide a window width the influence of noise becomes large and leads to larger reconstruction errors. Too small a window width however produced distortions at the peak $t = \tau$. We used the suggestion provided in reference [41] and chose a window width of about $\tau/3$. Concatenation and integration methods were used to retrieve the spectral phase and there was no significant difference. The reconstructed phase for the test pulse is shown in figure 7.12

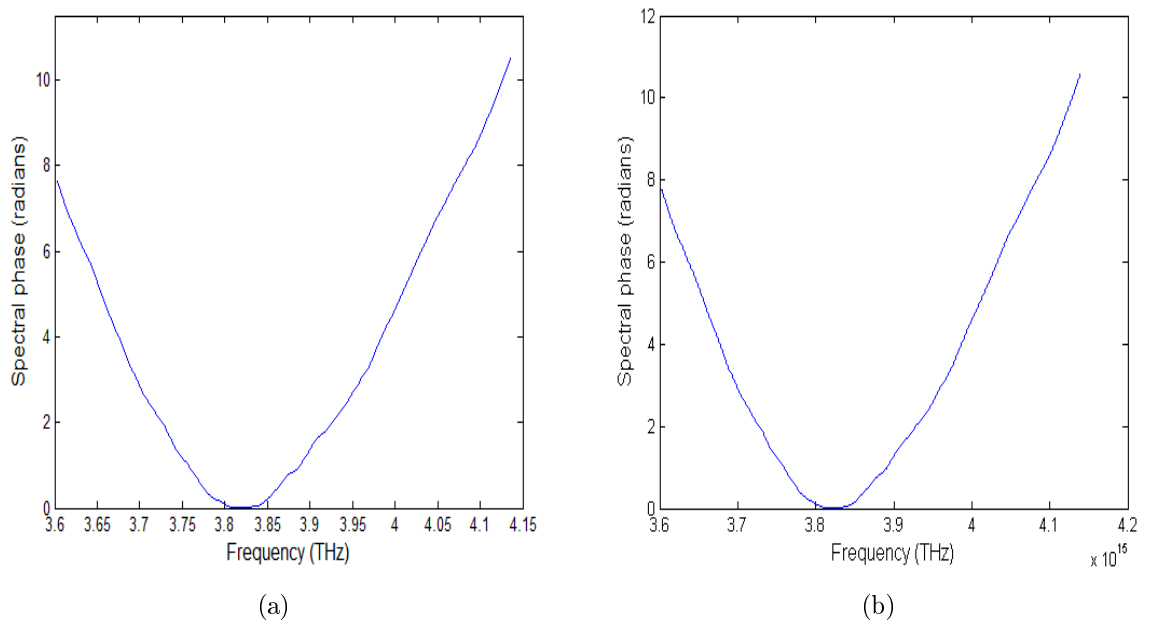


Figure 7.12: Reconstructed spectral phase using integration (a) and concatenation methods (b)

An online retrieval of the spectral amplitude was done. That is, the Dc peak in the Fourier transform of the interferogram was filtered using a super Gaussian centred around 0, this was then Fourier transformed back to frequency space. The temporal profile was retrieved by Fourier transforming the combined spectral amplitude and phase. The temporal phase is then the

argument of the complex temporal field. The retrieved spectral intensity and spectral phase, with its temporal profile and time dependent phase is shown in figure 7.13 and 7.14. The reconstructed temporal profile has a full width at half maximum of 106 fs.

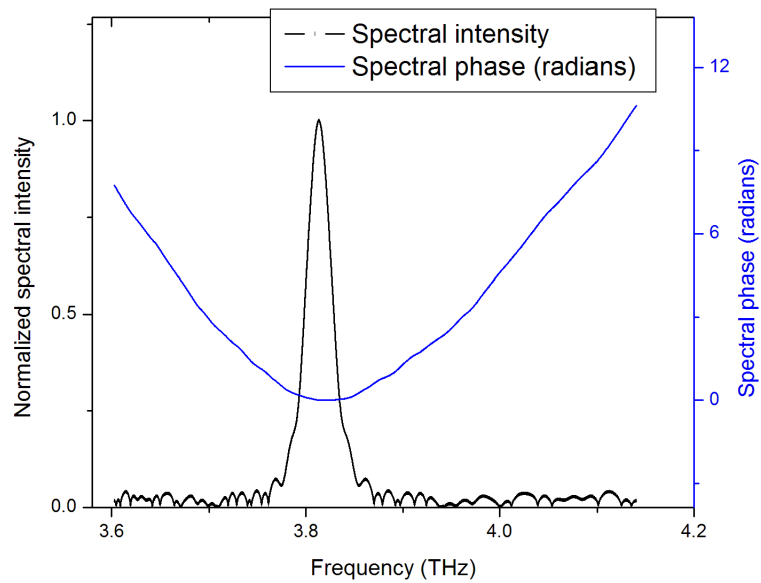


Figure 7.13: Retrieved spectral intensity and spectral phase

The spectral phase of a test pulse retrieved through the SPIDER algorithm and the same spectral phase of the test pulse after propagating through 1 mm glass plate is compared in figure 7.15. The phases of the two pulses are shifted with respect to each as expected [42].

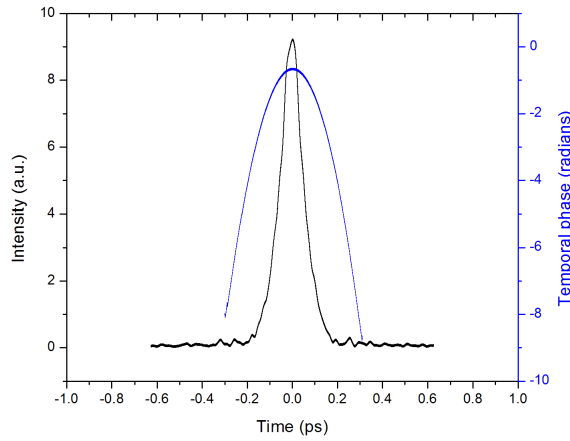


Figure 7.14: Retrieved temporal profile and time dependent phase

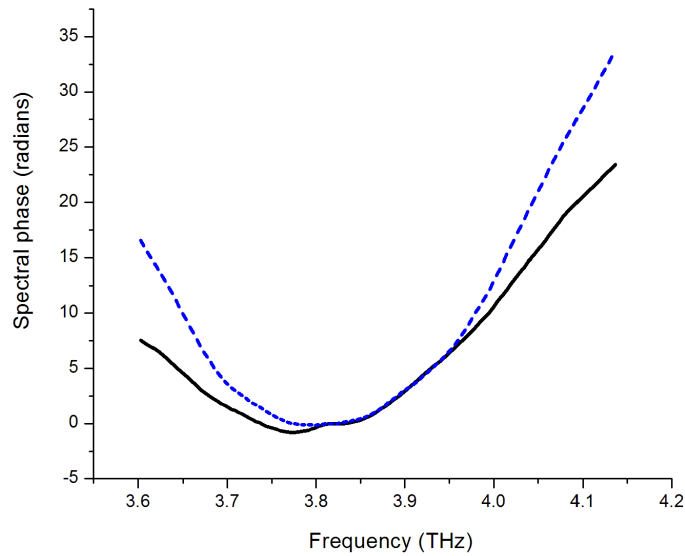


Figure 7.15: Spectral phase returned by SPIDER (straight line) for an input pulse similar to that shown in figure 7.7, and the same pulse after propagating through a glass of 1 mm thickness (dots)

7.4 Numerical simulations

It was important to verify the validity of the SPIDER algorithm used to retrieve the experimental data. A numerical simulation running in Matlab

was developed by modifying an existing code gotten from [43]. A theoretical short pulse was defined, with an input full width at half maximum of 80 fs and the input spectral phase was given by a fourth-order polynomial of the form

$$\phi(\omega) = a(\omega - \omega_0)^2 + b(\omega - \omega_0)^3 + c(\omega - \omega_0)^4 \quad (7.18)$$

where a , b and c are the quadratic, cubic and quartic components of the spectral phase [41]. The simulation showed that the SPIDER technique is ideal for retrieving fairly complicated pulse shapes. Figures 7.18, 7.19, and 7.20 shows the input and retrieved spectral phases using SPIDER, we assumed Gaussian pulse shape for the input pulse profiles.

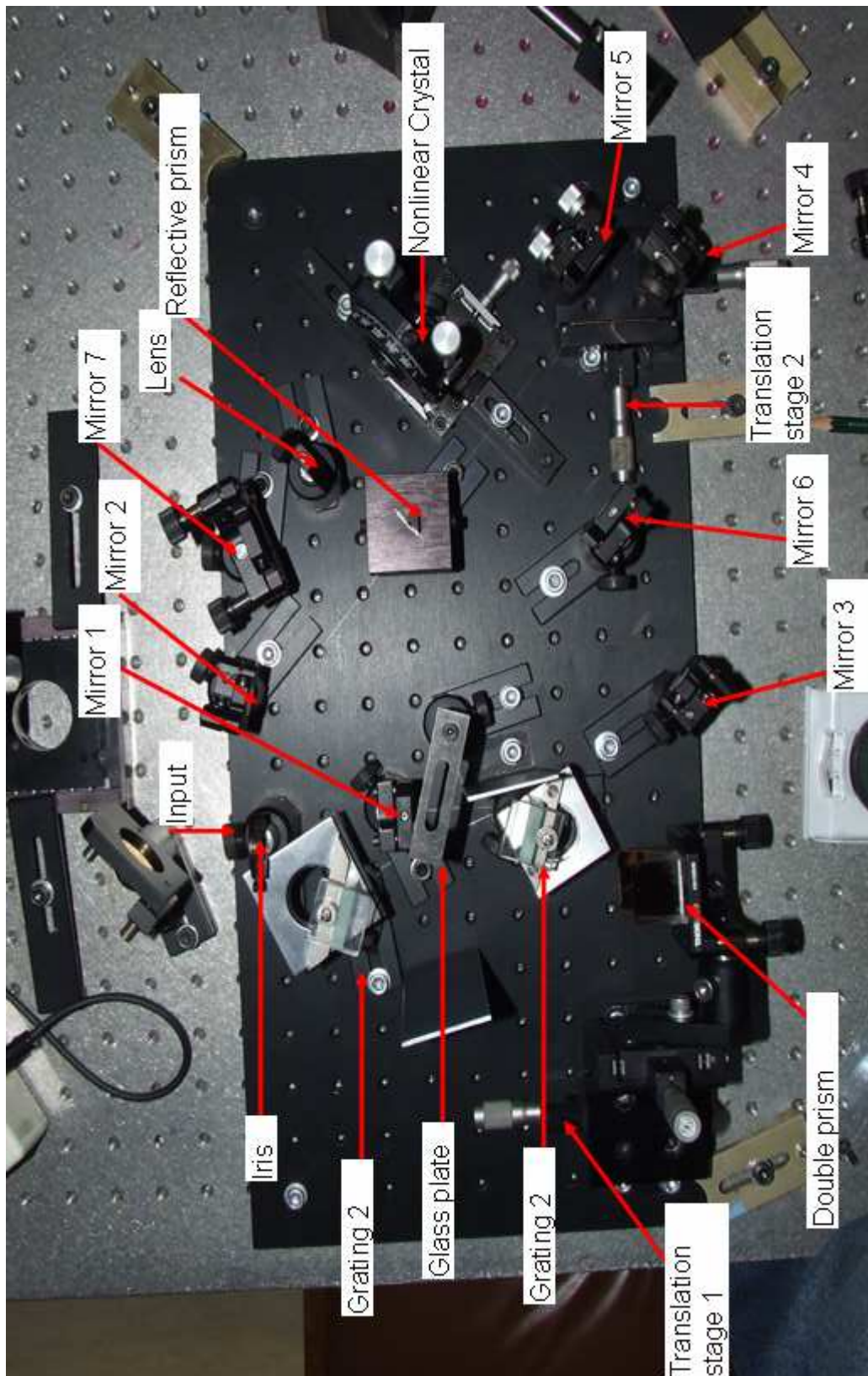


Figure 7.16: A picture of the SPIDER setup

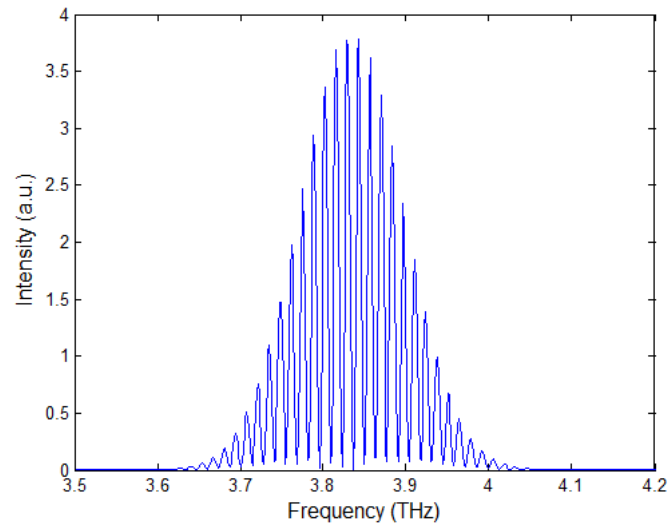
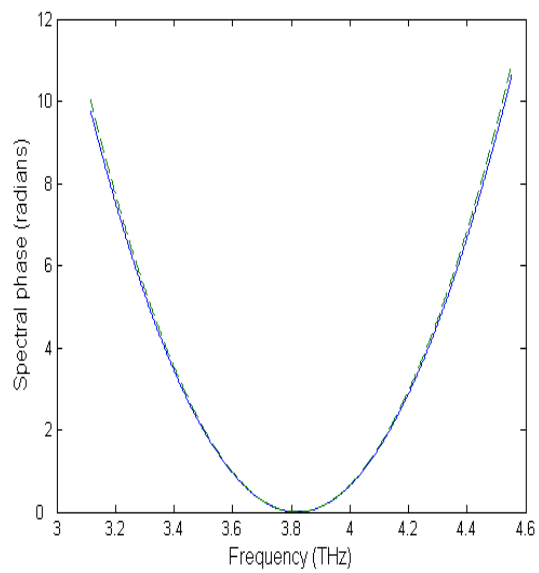


Figure 7.17: Simulated SPIDER interferogram

Figure 7.18: Input (dash line) and reconstructed quadratic phase (solid line) using the SPIDER algorithm, $a = 5 \times 10^{-20} \text{ fs}^2$, $b = 0$, and $c = 0$

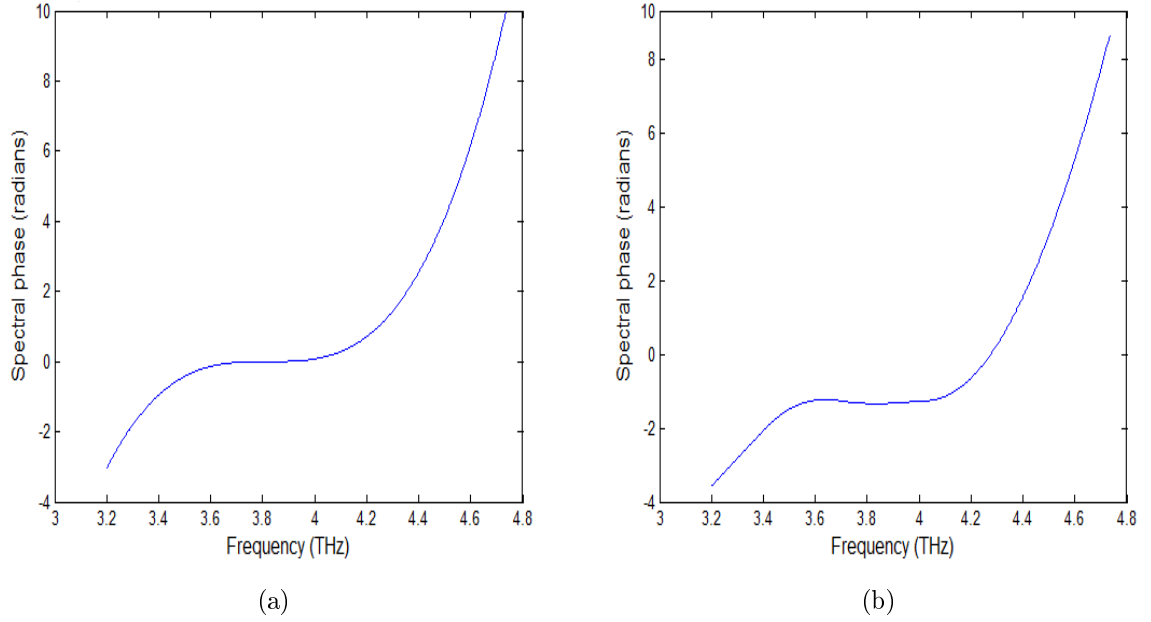


Figure 7.19: Input and reconstructed cubic phase using the SPIDER algorithm, $a = 0$, $b = 5 \times 10^{-56} \text{ fs}^2$, and $c = 0$

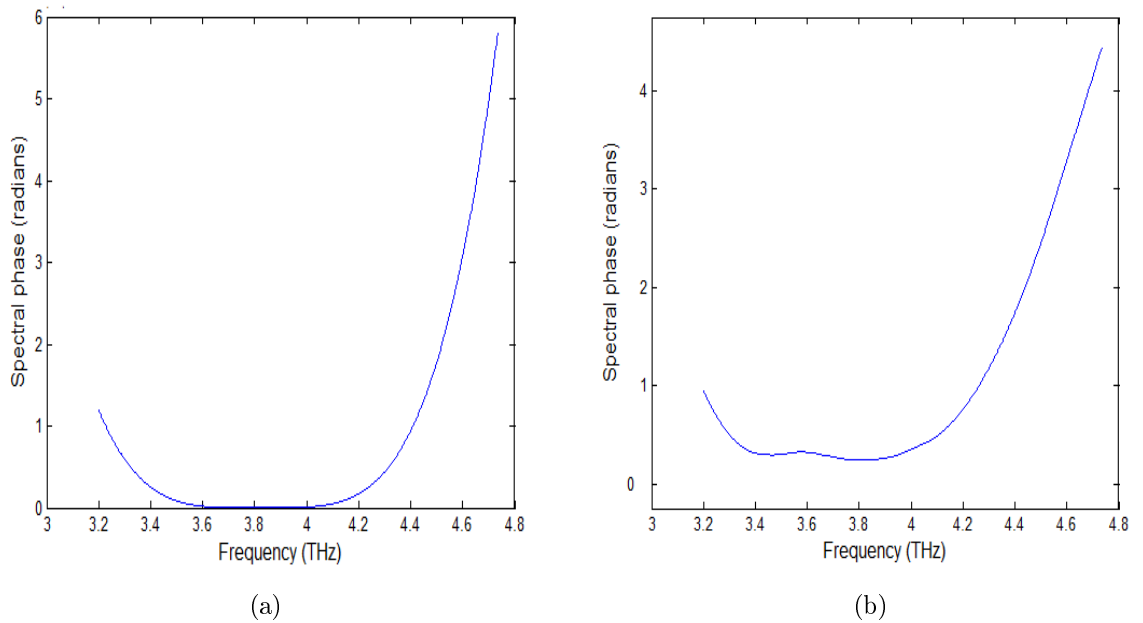


Figure 7.20: Input and reconstructed quartic phase using the SPIDER algorithm, $a = 0$, $b = 0$, and $c = 5 \times 10^{-71} \text{ fs}^2$

8. Conclusions

In this thesis, the concept of ultrashort pulse characterization have been studied. This work included theory, experiments, analysis of results and numerical simulations. In the theory we explained the traditional correlation techniques used for ultrashort pulse characterization and the theory of the SPIDER technique. Experimentally we constructed a SPIDER device and used it to characterize laser pulses emerging from a Ti:sapphire oscillator. Analysis of the experimental data obtained revealed that the pulse has a width of about 106 fs with a linear chirp. This chirp may be as a result of material dispersion in the output coupler of the laser, air, lenses etc. We evaluated the SPIDER technique by simulation. This involved defining a theoretical Gaussian shaped pulse with known phases and applying the inversion routine. The check was to see if the input spectral phase can be extracted and this was successful.

The advantages of the SPIDER technique over other self referencing schemes is its robustness to bandwidth effects, real-time and single shot capability [44]. The critical parameters that need to be optimized in the SPIDER algorithm are the number of points resolved by the spectrometer, the magnitude of the spectral shear, the delay between the replicas, and the width of the window used to isolate the side lobe of the Fourier transformed SPIDER interferogram. These effects were investigated using the simulated SPIDER algorithm. The SPIDER technique demonstrated in this work is the conventional method and it was adequate to characterize the available laser system. This conventional technique is not ideal for characterizing longer pulses from the picosecond range due to the limitations on the delay between the replicas and the spectrometer resolution. Another limitation of the SPIDER technique is its high sensitivity to alignment. Also, since this technique is based on a nonlinear process it can only be used to characterize pulses with high enough intensities.

Over the years different variants of the SPIDER technique has been demonstrated to optimize various parameters. For example, the zero-additional-

phase variant of SPIDER (ZAP-SPIDER) generates a shear by up-converting two strongly chirped pulses with a short test pulse. This solves the problem of the additional phase on one of the pulse replicas introduced through the material dispersion of the etalon or coating of the beam splitter in the conventional SPIDER technique [45]. In the standard SPIDER technique used in this work, the delay and the shear are linked and cannot be adjusted independently and therefore does not provide sufficient degrees of freedom to optimize these parameters [9]. The ZAP-SPIDER variant and Homodyne optical technique (HOT-SPIDER) allows for an independent adjustment of the delay and shear, this is critical when characterizing short pulses with spectral width close to the Fourier limit.

Appendix A.

A.1 Gaussian pulse propagation through a medium

Recall that the time-frequency relationship of Gaussian envelope pulse can be written as

$$E(z, t) = \int_{-\infty}^{\infty} E(z, \omega) e^{i\omega t} d\omega \quad (\text{A.1})$$

using the first three terms in the expansion of the propagation vector k , $E(z, \omega)$ is

$$E(z, \omega) = \exp \left[-ik(\omega_0)z - ik'z(\omega - \omega_0) - \frac{1}{4} \left(\frac{1}{a_0} + 2ik''z \right) (\omega - \omega_0)^2 \right] \quad (\text{A.2})$$

then

$$E(z, t) = \int_{-\infty}^{\infty} \exp \left[-ik(\omega_0)z - ik'z(\omega - \omega_0) - \frac{1}{4} \left(\frac{1}{a_0} + 2ik''z \right) (\omega - \omega_0)^2 \right] e^{i\omega t} d\omega \quad (\text{A.3})$$

insert $i\omega_0 t - i\omega_0 t$ into the exponent (this value is zero, but will help us with the solving)

$$E(z, t) = \int_{-\infty}^{\infty} \exp \left[i\omega_0 t - i\omega_0 t - ik(\omega_0)z - ik'z(\omega - \omega_0) - \frac{1}{4} \left(\frac{1}{a_0} + 2ik''z \right) (\omega - \omega_0)^2 \right] e^{i\omega t} d\omega \quad (\text{A.4})$$

Factorising the carrier frequency time and space dependence we get

$$\begin{aligned}
E(z, t) &= \int_{-\infty}^{\infty} \exp [i(\omega_0 t - k(\omega_0)z)] \\
&\times \exp \left[-\frac{1}{4} \left(\frac{1}{a_0} + 2ik''z \right) (\omega - \omega_0)^2 - i\omega_0 t - ik'z(\omega - \omega_0) \right] e^{i\omega t} d\omega \\
&= \exp [i(\omega_0 t - k(\omega_0)z)] \\
&\times \int_{-\infty}^{\infty} \exp \left[-\frac{1}{4} \left(\frac{1}{a_0} + 2ik''z \right) (\omega - \omega_0)^2 - i\omega_0 t - ik'z(\omega - \omega_0) + i\omega t \right] \times d\omega \\
&= \exp [i(\omega_0 t - k(\omega_0)z)] \\
&\times \int_{-\infty}^{\infty} \exp \left[-\frac{1}{4} \left(\frac{1}{a_0} + 2ik''z \right) (\omega - \omega_0)^2 + i(\omega - \omega_0)t - ik'z(\omega - \omega_0) \right] d\omega \\
&= \exp [i(\omega_0 t - k(\omega_0)z)] \\
&\times \int_{-\infty}^{\infty} \exp \left[-\frac{1}{4} \left(\frac{1}{a_0} + 2ik''z \right) (\omega - \omega_0)^2 + i(\omega - \omega_0)(t - k'z) \right] d\omega \quad (\text{A.5})
\end{aligned}$$

Recall that, $d\omega = d(\omega - \omega_0)$ since the center frequency ω_0 is a constant.

Letting

$$\frac{1}{a_0} + 2ik''z = \frac{1}{a(z)}$$

which describes the effect of the character of the medium and the distance through which the pulse travels on the pulse shape. Then an analytical expression is obtained for $E(z, t)$ as

$$\begin{aligned}
E(z, t) &= \frac{\exp [i(\omega_0 t - k(\omega_0)z)]}{2\pi} \\
&\times \int_{-\infty}^{\infty} \exp \left[-\frac{1}{4a(z)} (\omega - \omega_0)^2 + i(\omega - \omega_0)(t - k'z) \right] d\omega \quad (\text{A.6})
\end{aligned}$$

A.2 Conversion efficiency of the second harmonic wave

From Maxwell's equation, the wave equation for a non conducting medium is

$$\nabla^2 E - \epsilon_0 \mu_0 \frac{\partial^2 E}{\partial t^2} = \mu_0 \frac{\partial^2 P}{\partial t^2} \quad (\text{A.7})$$

We can then deduce that the second-harmonic term in the nonlinear polarisation P should generate a second-harmonic contribution to the electric field E . This means that an electric field of frequency ω in a non-centrosymmetric medium, will through the nonlinear polarization $P_{2\omega}$ generate an electric field at the second-harmonic frequency 2ω . Let us try to derive the intensity of the electric field at the second-harmonic frequency. We write the second-harmonic field as

$$E = \frac{1}{2} [E_{2\omega}(z)e^{-i(2\omega t - k_{2\omega}z)} + E_{2\omega}^*(z)e^{i(2\omega t - k_{2\omega}z)}] \quad (\text{A.8})$$

where $k_{2\omega} = \frac{2\omega}{c}\eta(2\omega)$ and $\eta(2\omega) = (\epsilon_{2\omega}/\epsilon_0)^{1/2}$ is the refractive index of the medium for radiation of frequency 2ω . The wave equation for the second-harmonic generation can then be derived. The first term in the left hand side of equation (A.7) becomes

$$\nabla^2 E_{2\omega} = \frac{1}{2} \left[\left(\frac{d^2 E_{2\omega}}{dz^2} + ik_{2\omega} \frac{dE_{2\omega}}{dz} \right) + ik_{2\omega} \left(\frac{dE_{2\omega}}{dz} - k_{2\omega}^2 E_{2\omega} \right) \right] e^{-i(2\omega t - k_{2\omega}z)} + c.c. \quad (\text{A.9})$$

Assuming the amplitude $E_{2\omega}$ to be slowly varying in z we make an approximation by neglecting second derivatives of $E_{2\omega}$, to get

$$\nabla^2 E_{2\omega} = \frac{1}{2} \left(2ik_{2\omega} \frac{dE_{2\omega}}{dz} - k_{2\omega}^2 E_{2\omega} + c.c. \right) \quad (\text{A.10})$$

which together with

$$\epsilon_0 \mu_0 \frac{\partial^2 E_{2\omega}}{\partial t^2} = -2\epsilon_0 \mu_0 \omega^2 [E_{2\omega} e^{-i(2\omega t - k_{2\omega}z)} + c.c.] \quad (\text{A.11})$$

gives the left side of equation (A.7) as

$$\nabla^2 E_{2\omega} - \epsilon_0 \mu_0 \frac{\partial^2 E_{2\omega}}{\partial t^2} \approx \left(ik_{2\omega} \frac{dE_{2\omega}}{dz} - \frac{1}{2} (k_{2\omega}^2 - 4\epsilon_0 \mu_0 \omega^2) E_{2\omega} \right) \times e^{-i(2\omega t - k_{2\omega} z)} + c.c \quad (\text{A.12})$$

For the second-harmonic field equation in (A.8), the right side of equation (A.7) has both linear (L) and nonlinear (NL) contributions at frequency 2ω :

$$P = \frac{1}{2} [P_{2\omega}^{(L)}(z) e^{i(2\omega t - k_{2\omega} z)} + P_{2\omega}^{(L)*}(z) e^{i(2\omega t - k_{2\omega} z)} + P_{2\omega}^{(NL)}(z) e^{2i(\omega t - k_{\omega} z)} + P_{2\omega}^{(NL)*}(z) e^{2i(\omega t - k_{\omega} z)}] \quad (\text{A.13})$$

and

$$\mu_0 \frac{\partial^2 P}{\partial t^2} = -2\mu_0 \omega^2 [P_{2\omega}^{(L)}(z) e^{i(2\omega t - k_{2\omega} z)} + P_{2\omega}^{(L)*}(z) e^{i(2\omega t - k_{2\omega} z)}] - 2\mu_0 \omega^2 [P_{2\omega}^{(NL)}(z) e^{2i(\omega t - k_{\omega} z)} + P_{2\omega}^{(NL)*}(z) e^{2i(\omega t - k_{\omega} z)}] \quad (\text{A.14})$$

Combining the real parts of equations (A.12) and (A.14), we get

$$\left(ik_{2\omega} \frac{dE_{2\omega}}{dz} - \frac{1}{2} (k_{2\omega}^2 - 4\epsilon_0 \mu_0 \omega^2) E_{2\omega} \right) e^{-i(2\omega t - k_{2\omega} z)} = -2\mu_0 \omega^2 P_{2\omega}^L(z) e^{i(2\omega t - k_{2\omega} z)} - 2\mu_0 \omega^2 P_{2\omega}^{NL}(z) e^{2i(\omega t - k_{\omega} z)} \quad (\text{A.15})$$

We know that $P^{(L)} = \epsilon_0 \chi E$, which at a frequency of 2ω becomes

$$P_{2\omega}^{(L)} = \epsilon_0 \chi(2\omega) E_{2\omega} \quad (\text{A.16})$$

and

$$k_{2\omega}^2 = (2\omega)^2 \epsilon_{2\omega} \mu_0 = 4\omega^2 \epsilon_0 \mu_0 \eta^2(2\omega) = 4\omega^2 \epsilon_0 \mu_0 [1 + \chi(2\omega)] \quad (\text{A.17})$$

We have also used the relation; speed of light in vacuum $c = \frac{1}{\sqrt{\mu_0 \epsilon_0}}$ and the speed of light in a medium at frequency 2ω is $v_{2\omega} = \frac{1}{\sqrt{\epsilon_{2\omega} \mu_0}}$.

We have taken $\chi_{2\omega}$ to be real because we are assuming absorption and other

loss processes to be negligible. The use of these relations in equation (A.15) results in the equation

$$ik_{2\omega} \frac{dE_{2\omega}}{dz} e^{i(2\omega t - k_{2\omega} z)} = -2\mu_0 \omega^2 P_{2\omega}^{NL}(z) e^{2i(\omega t - k_{\omega} z)} \quad (\text{A.18})$$

or

$$\begin{aligned} \frac{dE_{2\omega}}{dz} &= \frac{2i\mu_0 \omega^2}{k_{2\omega}} P_{2\omega}^{(NL)} e^{i(2\omega t - k_{2\omega} z - 2\omega t + 2k_{\omega} z)} \\ &= i\omega \sqrt{\mu_0 / \epsilon_{2\omega}} P_{2\omega}^{(NL)} e^{i(2k_{\omega} - k_{2\omega})z} \end{aligned} \quad (\text{A.19})$$

and this relates the second-harmonic field to the nonlinear polarization. Finally it is convenient to define a quantity

$$P_{2\omega}^{(NL)} = dE_{\omega}^2(z) \quad (\text{A.20})$$

where d represents

$$d = \epsilon_0 \chi^{(2)}(2\omega, \omega, \omega) \quad (\text{A.21})$$

Thus we can write equation (A.19) as

$$\frac{dE_{2\omega}}{dz} = i\omega \sqrt{\frac{\mu_0}{\epsilon_{2\omega}}} dE_{\omega}^2(z) e^{i\Delta k z} \quad (\text{A.22})$$

where

$$\Delta k = 2k_{\omega} - k_{2\omega} = 2\omega \sqrt{\epsilon_0 \mu_0} [\eta(\omega) - \eta(2\omega)] \quad (\text{A.23})$$

The solution to equation (A.22) gives the second-harmonic field amplitude $E_{2\omega}(z)$. In order to solve the equation, we need to know $E_{\omega}(z)$. To simplify our work, we make the approximation that there is little attenuation of the fundamental wave so that E_{ω} is a constant

$$E_{\omega}(z) \approx E_{\omega}(0) \quad (\text{A.24})$$

This approximation is often called *small signal limit*. Within this approximation, the signal of the second-harmonic wave generated is still small. In practice as the conversion from a fundamental to a second-harmonic wave continues in the medium, there is depletion of the fundamental wave and this approximation is no longer a good one.

With this approximation (A.22) can be integrated to obtain

$$E_{2\omega}(z) \approx i\omega \sqrt{\frac{\mu_0}{\epsilon_{2\omega}}} dE_{\omega}^2(0) \int_0^z e^{i\Delta kz} dz \quad (\text{A.25})$$

$$= i\omega \sqrt{\frac{\mu_0}{\epsilon_{2\omega}}} dE_{\omega}^2(0) \left(\frac{1}{i\Delta k} (e^{i\Delta kz} - 1) \right) \quad (\text{A.26})$$

Now $\frac{1}{i\Delta k}(e^{i\Delta kz} - 1)$ can be written as

$$\frac{1}{i\Delta k}(e^{i\Delta kz} - 1) = \frac{e^{i\Delta kz/2}}{i\Delta k} (e^{i\Delta kz/2} - e^{-i\Delta kz/2}) \quad (\text{A.27})$$

equation (A.27) becomes

$$\frac{1}{i\Delta k}(e^{i\Delta kz} - 1) = 2e^{i\Delta kz/2} \frac{1}{\Delta k} \sin \frac{1}{2} \Delta kz \quad (\text{A.28})$$

$$= ze^{i\Delta kz/2} \left(\frac{\sin \frac{1}{2} \Delta kz}{\frac{1}{2} \Delta kz} \right) \quad (\text{A.29})$$

So with the approximation that the fundamental wave is unattenuated we have

$$E_{2\omega}(z) = i\omega \sqrt{\frac{\mu_0}{\epsilon_{2\omega}}} dE_{\omega}^2(0) ze^{i\Delta kz/2} \left(\frac{\sin \frac{1}{2} \Delta kz}{\frac{1}{2} \Delta kz} \right) \quad (\text{A.30})$$

equation (A.30) describes the amplitude of the second-harmonic wave, under the approximation that the applied field is not attenuated inside the medium.

Suppose the nonlinear crystal is of length L as in Figure (2.3) . The second-harmonic field at the exit face of the crystal is then given by equation (A.30)

with $z = L$. Thus equation (A.30) implies that

$$|E_{2\omega}(L)|^2 = \frac{\mu_0\omega^2}{\epsilon_{2\omega}} |E_\omega(0)|^4 L^2 \left(\frac{(\sin\frac{1}{2})\Delta kL}{\frac{1}{2}\Delta kL} \right). \quad (\text{A.31})$$

The intensities of the fields at ω and 2ω are given by [1]

$$I_\omega = \frac{1}{2} \sqrt{\frac{\epsilon_\omega}{\mu_0}} |E_\omega|^2, \quad (\text{A.32})$$

$$I_{2\omega} = \frac{1}{2} \sqrt{\frac{\epsilon_{2\omega}}{\mu_0}} |E_{2\omega}|^2. \quad (\text{A.33})$$

It follows from (A.31) that

$$\begin{aligned} I_{2\omega}(L) &= \frac{2\mu_0^{3/2} d^2 \omega^2}{\epsilon_\omega \sqrt{\epsilon_{2\omega}}} |E_\omega(0)|^4 \frac{1}{4} \epsilon_\omega / \mu_0 L^2 \left(\frac{\sin\frac{1}{2}\Delta kL}{\frac{1}{2}\Delta kL} \right)^2 \\ &= \frac{2\mu_0^{3/2} d^2 \omega^2}{\epsilon_\omega \sqrt{\epsilon_{2\omega}}} I_\omega^2(0) L^2 \left(\frac{\sin\frac{1}{2}\Delta kL}{\frac{1}{2}\Delta kL} \right)^2 \\ &= 2 \left(\frac{\mu_0}{\epsilon_0} \right)^{3/2} \frac{\omega^2 d^2}{\eta^2(\omega)\eta(2\omega)} I_\omega^2(0) L^2 \left(\frac{\sin\frac{1}{2}\Delta kL}{\frac{1}{2}\Delta kL} \right)^2. \quad (\text{A.34}) \end{aligned}$$

This equation gives the intensity of the second-harmonic wave under the approximation that the fundamental wave is unattenuated in the medium, and as expected, the intensity of the second-harmonic wave is seen to increase as the square of the intensity of the fundamental wave. Since the phase velocities of the fundamental and second-harmonic wave are different, the second-harmonic wave do not receive enough energy from the fundamental wave so the approximation that the wave is unattenuated is fair at this point.

From this we can now obtain the power conversion efficiency for second-

harmonic generation, C_{SHG} as

$$C_{SHG} = \frac{I_{2\omega}(L)}{I_{\omega}(0)} \quad (\text{A.35})$$

$$= 2 \left(\frac{\mu_0}{\epsilon_0} \right)^{3/2} \frac{\omega^2 d^2}{\eta^2(\omega)\eta(2\omega)} I_{\omega}(0) L^2 \left(\frac{\sin \frac{1}{2} \Delta k L}{\frac{1}{2} \Delta k L} \right)^2. \quad (\text{A.36})$$

We see in equation (A.36) that the conversion efficiency of the second-harmonic generation is maximized when $\Delta k = 0$. This leads to the requirement of phase matching that makes $\Delta k = 0$. When phase matching is achieved, the conversion efficiency of the second-harmonic generation increases, in other words, there is transfer of energy from the fundamental to the second-harmonic wave and we can no longer neglect the depletion of the fundamental wave. As a result of this depletion, the second-harmonic generation reaches a saturation point where it maintains a constant value, this occurs because the source of its energy which is from the fundamental wave is depleted.

A.3 Matlab code for the phase retrieval

```
%Fourier transform of the frequency space
function t = wspace(w,nw);

if (nargin<2)
    nw = length(w);
    dw = w(2) - w(1);
    w = w(nw) - w(1) + dw;
end

if (nargin == 2)
    dw = w/nw;
end

t =2* pi*(-nw/2:nw/2-1)'/w;
```

```
kv = find(w >= pi/dw);
t(kv) = t(kv) - 2*pi/dw;

F=load('spider.txt'); %Load the experimental data for the SPIDER trace
A=load('secondharmonic.txt'); %Load the experimental data obtained
for the second harmonic generated of the unsheared replica
C=load('fundamental.txt'); %Load the experimental data for the
fundamental spectrum
wavelength0=C(:,1).*1e-9; % Use actual value in nanometers
(fundamental spectrum data)

wavelength=A(:,1).*1e-9; %F=load('spider.txt'); %Load the experimental
data for the SPIDER trace
A=load('secondharmonic.txt'); %Load the experimental data obtained
for the second harmonic generated of the unsheared replica
C=load('fundamental.txt'); %Load the experimental
data for the fundamental spectrum
wavelength0=C(:,1).*1e-9; % Use actual value in nanometers
(fundamental spectrum data)

wavelength=A(:,1).*1e-9; %Use actual value in nanometers (SHG data)

wavelength1=F(:,1).*1e-9; %Use actual value in nanometers (SPIDER data)

y=A(:,2);
z=F(:,2);
z2=C(:,2);
\chapter{}
\section{Phase reconstruction algorithm}
c=3e8;
w=2*pi*c./wavelength; %Conversion to frequency
ws=2*pi*c./wavelength1; %Conversion to frequency
```

```

rws=2*pi*c./rw           %Conversion to frequency

figure (1)
plot(wavelength,y,'LineWidth',1); %Plot wavelength
versus spectral intensity of the SH trace
figure (2)
plot(wavelength1,z,'LineWidth',1);%Plot wavelength
versus spectral intensity of the SH trace

figure (3)

plot(w,y,'LineWidth',1);           %Plot frequency versus spectral
intensity of the SH trace
figure (4)

plot(ws,z,'LineWidth',1);           %Plot frequency versus spectral
intensity of the SPIDER trace

B=fft(y); %Take fast Fourier transform of the SH spectral intensity
Bs=fft(z); %Take fast Fourier transform of the SPIDER spectral intensity

figure (5)
%Plot the inverse Fourier transform of the SH interference spectra
plot(wspace(w),(abs(fftshift(B))), 'LineWidth',1);
figure (6)
%Plot the inverse Fourier transform of the SPIDER
plot(wspace(ws),(abs(fftshift(Bs))), 'LineWidth',1); interferogram
b1=-290*log(2)/(1.4e-12)^4;
b=-290*log(2)/(1.4e-12)^4;
H=abs(exp(b*(wspace(w)-(1.4e-12)).^(4))); %(Defining super gaussian filters)
HE=abs(exp(b1*(wspace(ws)).^(4)));
Hs=abs(exp(b*(wspace(ws)-(1.4e-12)).^(4)));

```

```
figure (7)
plot(wspace(w),abs(fftshift(B)),wspace(w),H,'LineWidth',1);%
figure (8)
plot(wspace(ws),abs(fftshift(Bs)),wspace(ws),Hs,'LineWidth',1);%
fg=H.*abs(fftshift(B));          % Select positive side band
fgs=Hs.*abs(fftshift(Bs));
figure (9)
plot(wspace(w),(fg),'LineWidth',1)
figure (10)
plot(wspace(ws),(fgs),'LineWidth',1)

figure (11)
k=fft(fg)
plot(w,((abs(fftshift(k)))),'LineWidth',1); % Fourier transform the selected
side band to frequency (SPIDER trace)
figure (12)
ks=fft(fgs)
plot(ws,((abs(fftshift(ks)))),'LineWidth',1);% Fourier transform the s
elected side band to frequency (SH trace)

%j=abs(fftshift(k));
%figure(13)
o=(angle((conj(k))));          % Retrieve the argument of the Fourier
transform of the selected side band
%plot(w,o,'LineWidth',1)
figure(14)
os=(angle((conj(ks))));          % Retrieve the argument of the Fourier
transform of the selected side band
plot(ws,os,'LineWidth',1)

%figure(15)
%plot(w,unwrap(o))
figure (16)
```

```

o3=(os-(o));
o4=unwrap(angle(ks.*conj(k))); % Unwrap phase and subtract calibration
plot(ws,o4)
sh=5e12;      %Shear
s=ws-sh/2;
phi=cumtrapz(w,(o4-spline(s,o4,4.864e15))/sh);% Integrate phase via
    trapezium (mid-point) rule
phi = phi - spline(s, phi, 4.864e15);
figure (17)
phio=(phi/100);
plot((ws/2)/2*pi,phi/100);
omega_c = (min(w):abs(sh):max(w))';

phi_c = cumsum(spline(w, o4, omega_c)...
    -spline(s, o4, 4.864e15));          % Concatenate phase
removing linear phase
phi_c = phi_c - spline(omega_c, phi_c, 4.864e15);
figure(18)
plot((omega_c/2)/2*pi,phi_c/100);
figure(19)
plot(rws,z2)
figure (20)
plot(wspace(ws),(fgE),'LineWidth',1)
kE=fft(fgE)
figure (21)
%Online retrieval of the spetral amplitude
EW=sqrt(abs(fftshift(kE))/max(abs(fftshift(kE))));
plot(ws,EW);

dw = sh;
Nw=2048;
w1 = (0:Nw-1)*dw;
Nt = 2048;

```

```

dt = 2*pi/(Nt*dw);
t = ((0:Nt-1)'-(Nt/2))*dt;

fw = (w1>=min(ws)).*(w1<=max(ws));%Interpolate data onto linear freq grid
phi_=spline(ws, phio, w1).*fw;
EW_=spline(ws, EW, w1).*fw;
EWreal=EW_.*exp(i*(phi_));
figure(22)
plot(w1,abs(EWreal));
figure(23)
Etreal=fftshift(fft(EWreal,Nt));% Temporal profile
%Temporal phase

s1=(ws/2)/2*pi;
figure (24)
plot (w1,phi_);
phit=angle((Etreal))-(w1).*t;
figure (25)
plot (t,unwrap(phit)/100)

```

A.4 SPIDER verification algorithm

```

C = 299.792458; %Speed of light (nm/fs)
%Coefficients for the third order polynomial
a =0;
b=0;
c=0;
s=50;
tau = 200;           %delay between replicas
TLP = 80;           %Transform limited (FTL) FWHM
intensity pulse duration (fs)

```

```

shear = 2*pi/(10*Dt);      % Maximum pulse window width is 10*TLP
changew2freq = @(x) 2*pi*C./x; %Change wavelenght in nm to
angular frequency

% Gaussian function:
%     x   =   Co-ordinate
%     x0  =   Centre
%     dx  =   FWHM
%           = sqrt(2*log(2))*sigma_x, where sigma_x is 1/e^2 half width
%     n   =   Order (normal = 1)
gauss1D = @(x, x0, dx, n) exp(-log(2)*(2*(x-x0)/dx).^(2*abs(floor(n))));

Nw = 2024;                %Number of freq/wavelength data points

% Wavelength
lambda_min = 650;
lambda_max = 950;
dlambda = (lambda_max-lambda_min)/(Nw-1);
lambda = (0:Nw-1)*dlambda + lambda_min;

% Angular frequency
omega =(changew2freq(lambda));
omega_max = max(omega);
omega_min = min(omega);
domega = (omega_max-omega_min)/(Nw-1);

% Define the Gaussian pulse

sw = 4*log(2)/TLP;        % FWHM intensity bandwidth
(fs) for FTL duration TLP
lambda_0 = 800;           % Central wavelength (nm)
w0 = changew2freq(lambda_0); % Central angular frequency
%Define the third order polynomial (SH)

```

```

phi = s*(omega-w0)+a*(omega-w0).^2 + b*(omega-w0).^3 + c*(omega-w0).^4;

phi = phi - spline(omega, phi, w0);          % Remove absolute phase
%Define the third order polynomial for the SPIDER trace
phi_1 =s*(omega-w0)+ a*(omega-w0 + shear).^2 +
  b*(omega-w0 + shear).^3 + c*(omega-w0 + shear).^4;

phi_1 = phi_1 - spline(omega, phi_1, w0);
Ew = gauss1D(omega, w0, sqrt(2)*Dw, 1).*exp(i*phi);
  %Define Gaussian pulse replica without the shear in freq domain
Ew1 = gauss1D(omega, w0+shear, sqrt(2)*Dw, 1).*exp(i*(phi_1 + omega*tau ));
Int_spider = abs(Ew + Ew1).^2;
Int_cal = abs(Ew.*(1+exp(i*omega*tau))).^2;

omega_lin = (0:Nw-1)']*domega + omega_min;    % Generate linear freq grid
pxls = (1:Nw)';                             % pxl grid (for filter)
%inverse Fourier of the SPIDER and SH interferogram
It = fftshift(fft(Int_spider));
Itc = fftshift(fft(Int_cal));

%selecting the positive side band of the inverse Fourier transform and
%Fourier transform in back to frequency domain
ft = gauss1D(pxls,583,40, 4);
Iwf = ifft(ifftshift(It.*ft));
Iwcf = ifft(ifftshift(Itc.*ft));

%unwrap phase and subtract linear phase term
theta = unwrap(angle(Iwf.*conj(Iwcf)));

% New frequency ranges - this is because the reconstructed phase falls on
% the frequency grid between the two sheared pulses.

```

```

omega_s = omega-shear/2;
% Retrieving phase by integration (trapezium (mid-point) rule)
% Integrate (removing linear slope)
phi_i = cumtrapz(omega, (theta-spline(omega_s, theta, w0))/shear);
phi_i = phi_i - spline(omega_s, phi_i, w0); % Remove absolute phase
phi_i=phi_i/max(abs(phi_i))

%Using concatenation
omega_c = (omega_min:abs(shear):omega_max)';
phi_c = cumsum(spline(omega, theta, omega_c)...
    -spline(omega_s, theta, w0)); % Concatenate, removing linear phase
phi_c = phi_c - spline(omega_c, phi_c, w0); % Remove absolute phase

Ew_sp=abs(Ew)/max(abs(Ew)); % Using online retrieval of the spectral amplitude
dw = shear;
w = (0:Nw-1)'*dw;
Nt = 4096;
dt = 2*pi/(Nt*dw);
t = ((0:Nt-1)'-floor(Nt/2))*dt;
fw = (w>=omega_min).*(w<=omega_max);

Ew_sp_ = spline(omega, Ew_sp, w).*fw;
phi_i_ = spline(omega_s, phi_i, w).*fw;
phi_c_ = spline(omega_c, phi_c, w).*fw;

Ew_sp_p= Ew_sp_.*exp(i*phi_i_); %Combine spectral amplitude
with spectral phase
Et_sp_p= fftshift(fft(Ew_sp_p, Nt));

figure (1)
plot(omega, Int_spider)
figure (2)
plot (omega,phi_i)

```

Bibliography

- [1] Milonni P.W. and Joseph H.E. *Lasers*. Wiley Interscience Publication, New York, 1988.
- [2] Boyd R.W. *Nonlinear Optics*. Academic Press, Elsevier Science, 1992.
- [3] Claude Rulliere. *Femtosecond laser pulses, principles and experiments*. Springer Science+Business Media, Inc., 2005.
- [4] Mario Bertolotti. *The History Of The Laser*. IOP Publishing Ltd, 2005.
- [5] N. Bloembergen. From nanosecond to femtosecond science. *Reviews of Modern Physics*, 71(2), 1999.
- [6] Rick Trebino, Kenneth W. DeLong, David N. Fittinghoff, John N. Sweetser, Marco A. Krumbugel, and Bruce A. Richman. Measuring ultrashort laser pulses in the time-frequency domain using frequency-resolved optical gating. *Rev. Sci. Instrum.*, 68(9), 1997.
- [7] Christophe Dorrer and Manuel Joffre. Trends in femtosecond lasers and spectroscopy; characterization of the spectral phase of ultrashort light pulses. *C. R. Acad. Sci.*, t. 2, SÃ©rie IV:1415–1426, 2001.
- [8] Josh Thornes, Philip Poon, and Matthew E. Anderson. Complete characterization of femtosecond pulses using an all-electronic detector. *Opt. Soc. Am. B*, 21(7), 2004.
- [9] Jonathan R. Birge and Franz X. KÃ¼rtner. Analysis and mitigation of systematic errors in spectral shearing interferometry of pulses approaching the single-cycle limit [invited]. *J. Opt. Soc. Am. B*, 25(6), 2008.
- [10] Steffen Prein, Scott Diddams, and J.-C. Diels. Complete characterization of femtosecond pulses using an all-electronic detector. *Optics Communications*, 123:567–573, 1996.
- [11] P. N. Kean D. E. Spence and W. Sibbett. 60-fs pulse generation from a self-mode-locked Ti:sapphire laser. *Optics Express*, 16(1), 1991.

-
- [12] M.E Anderson, A Monmayrant, S.P Gorza P. Wasylczyk, and I.A. Wamsley. A decade of measuring ultrashort pulses. *Laser Phys. Lett.*, 2008.
- [13] Gavin D. Reid and Klaas Wynne. Ultrafast laser technology and spectroscopy. in encyclopedia of analytical chemistry.
- [14] Kelin J. Kuhn. *Laser Engineering*. Prentice-Hall, Inc., 1998.
- [15] Silfvast W.S., editor. *Laser Fundamentals*. Cambridge University Press, United States of America, 1996.
- [16] Grant R. Fowles. *Introduction to mordern optics*. Dover publications, 1989.
- [17] Jia-Ming Liu. *Photonic devices*. Cambridge University Press, New York, 2005.
- [18] Siegman E. Anthony. *Lasers*. University Science Books, United States of America, 1986.
- [19] Ian Wamsley, Leon Waxer, and Christopher Dorrer. The role of dispersion in ultra fast optics. *Review of Scientific Instruments*, 72(1), 2001.
- [20] David L. Andrews ad Andrey A. demidov. *An Introduction to LASER Spectroscopy*. Plenum press, New York, 1995.
- [21] Robert Guenther. *Modern Optics*. John Willey and sons, 1990.
- [22] W. Demtröder, editor. *Laser spectroscopy*. Springer-Verlag Belin Heidelberg, New York, 2003.
- [23] Jean-Claude Diels and Wolfgang Rudolph. *Ultrashort Pulse Laser Phenomena*. Elsevier Inc, 2006.
- [24] D. T. Reid, M. Padgett, C. McGowan, W. E. Sleat, and W. Sibbett. Light-emitting diodes as measurement devices for femtosecond laser pulses. *Optics Letters*, 22(4), 1997.

-
- [25] Jean-Claude M. Diels, Joel J. Fointaine, Ian C. McMichael, and Francesco Simoni. Control and measurement of ultrashort pulse shapes (in amplitude and phase with femtosecond accuracy). *Applied Optics*, 24(9), 1985.
- [26] F. Hache, T. J. Driscoll, M. Cavallari, and G. M. Gale. Measurement of ultrashort pulse durations by interferometric autocorrelation: influence of various parameters. *Applied Optics*, 35(18), 1996.
- [27] Christophe Dorrer, Nadia Belabas, Jean-Pierre Likforman, and Manuel Joffre. Spectral resolution and sampling issues in fourier-transform spectral interferometry. *Opt.Soc.Am.B*, 17(10), 2000.
- [28] Christophe Dorrer. Concepts for the temporal characterization of short optical pulses. *Eurasip Journal on Applied Signal Processing*, 10, 2005.
- [29] Christophe Dorrer, Nadia Belabas, Jean-Pierre Likforman, and Manuel Joffre. Experimental implementation of fourier-transform spectral interferometry and its application to the study of spectrometers. *Opt.Soc.Am.B*, 2000.
- [30] David N. Fittinghoff, Jason L. Bowie, John N. Sweetser, Richard T. Jennings, Marco A. Krumbugel, Kenneth W. DeLong, and Rick Trebino. Measurement of the intensity and phase of ultraweak, ultrashort laser pulses. *Optics Letters*, 21(12), 1996.
- [31] *Combustion Research Facility NEWS*, volume 18, Livermore, California, 1996.
- [32] I. G. Cormack, F. Baumann, and D. T. Reid. Measurement of group velocity dispersion using white light interferometry: A teaching laboratory experiment. *Am. J. Phys.*, 68(12), 2000.
- [33] Christophe Dorrer and Inuk Kang. Highly sensitive direct characterization of femtosecond pulses by electro-optic spectral shearing interferometry. *Optics Letters*, 28(6), 2003.

-
- [34] Christophe Dorrer Inuk Kang and Francesco Quochi. Implementation of electro-optic spectral shearing interferometry for ultrashort pulse characterization. *Optics Letters*, 28(22), 2003.
- [35] Antoine Monmayrant, Simon-Pierre Gorza, Piotr Wasylczyk, and Ian Walmsley. Beyond the fringe: SPIDER-the anatomy of ultrashort laser pulses. *Optical Metrology*, 2007.
- [36] Timothy M. Shuman, Matthew E. Anderson, Jake Bromage, Chris Iaconi, Leon Waxer, and Ian A. Walmsley. Real-time spider: ultrashort pulse characterization at 20 Hz. *Optics Express*, 5(6), 1999.
- [37] Franz X. Kärtner. *Few-Cycle Laser Pulse Generation and Its Applications*. springerlink.com, 2004.
- [38] Chris Iaconis and Ian A. Walmsley. Self-referencing spectral interferometry for measuring ultrashort optical pulses. *IEEE Journal of Quantum Electronics*, 35(5), 1999.
- [39] R. L. Fork, C. H. Brito, P. C. Becker, and C. V. Shank. Compression of optical pulses to six femtoseconds by using cubic phase compensation. *Optics Letters* 12, 12(7):483, 1987.
- [40] C. Dorrer, B. de Beauvoir, C. Le Blanc, J.-P. Rousseau, S. Ranc, P. Rousseau, J.-P. Chambaret¹, and F. Salin². Characterization of chirped-pulse amplification systems with spectral phase interferometry for direct electric-field reconstruction. *Appl. Phys.*, 70(S77-S84), 2000.
- [41] M.E. Anderson, L.E.E. de Araujo, E.M. Kosik, and I.A. Walmsley. The effects of noise on ultrashort-optical-pulse measurement using SPIDER. *Appl. Phys.*, 2000.
- [42] K. C. Chu, J. P. Heritage, R. S. Grant, K. X. Liu, and A. Dienes. Direct measurement of the spectral phase of femtosecond pulses. *Optics Letters*, 20(8), 1995.
- [43] <http://www.mathworks.com/matlabcentral/fileexchange/15657>.

-
- [44] Peter Baum, Stefan Lochbrunner, and Eberhard Riedle. Zero-addtional-phase SPIDER: full characterization of visible and sub-20-fs ultraviolet pulses. *Opt. Soc. Am. B*, 22(9), 2004.
- [45] Peter Baum and Eberhard Riedle. Design and calibration of zero-additional-phase SPIDER. *Opt. Soc. Am. B*, 22(9), 2004.